Geoacoustic Inversion of Subbottom Channels Using Multiple Frequency Input Parameters

by

Rebecca Weeks

A Thesis Submitted to the Faculty of

The College of Engineering and Computer Science

in Partial Fulfillment of the Requirements for the Degree of

Master of Science

Florida Atlantic University

Boca Raton, Florida

May 2010

Geoacoustic Inversion of Subbottom Channels Using Multiple Frequency Input Parameters
by

Rebecca Weeks

This thesis was prepared under the direction of the candidate's thesis advisor, Dr. George Frisk, Department of Ocean and Mechanical Engineering, and has been approved by the members of her supervisory committee. It was submitted to the faculty of the College of Engineering and Computer Science and was accepted in partial fulfillment of the requirements for the degree of Master of Science.

SUPERVISORY COMMITTEE:

George V. Frisk, Ph.D.
Thesis Advisor

Stewart Glegg, Ph.D.

Pierre Beaujean, Ph.D.

Kyle Becker, Ph.D.,
Pennsylvania State University

Mohammad Ilyas, Ph.D.
Interim Chair, Department of Ocean and Mechanical Engineering

Karl K. Stevens, Ph.D., P.E.
Dean, College of Engineering and Computer Science

Barry T. Rosson, Ph.D.
Dean, Graduate College

April 21, 2010
Date

ACKNOWLEDGEMENTS

I would like to thank my thesis advisor, Dr. George Frisk, for his support and guidance of my thesis work, and the members of my thesis committee, Stewart Glegg, Pierre-Phillipe Beaujean, and Kyle Becker. I also want to thank John Goff for providing the necessary data to make models for the inversions. I would also like to thank Cindy Sellers for all of her help during my summer at Woods Hole, and her willingness to help through phone and email while I was in Florida.

ABSTRACT

Author:	Rebecca Weeks
Title:	Geoacoustic Inversion of Subbottom Channels Using Multiple Frequency Input Parameters
Institution:	Florida Atlantic University
Thesis Advisor:	Dr. George V. Frisk
Degree:	Master of Science
Year:	2010

This thesis investigates inversion techniques used to determine the geoacoustic properties of a shallow-water waveguide. The data used were obtained in the Shallow Water ’06 Modal Mapping Experiment in which four buoys drifted over a system of subbottom channels. The method used was perturbative inversion using modal eigenvalues as input parameters, which were found using an autoregressive spectral estimator. This work investigates the differences between a “channel” region and a “no channel” region based on an inferred stratigraphic model. Inversions were performed on data from a single buoy both at individual frequencies and multiple frequencies simultaneously. Since the use of multiple frequencies and a certain set of constraints proved to be an effective method of inversion, the method was applied to data from the other three buoys as well. It is shown that the “channel” and “no channel” regions have significantly different sound speed profiles.

CONTENTS

TABLES

FIGURES

1.0 Introduction

1.1 Objectives

Sound waves in deep water environments propagate through a medium that is large, stable, and slowly varying, and bottom interaction is typically of secondary importance. However, in shallow water, the seafloor significantly interacts with and reflects the sound waves, which react differently to seafloors with different compositions. Research is being done to increase understanding of this shallow water acoustic propagation. The goals of this research at Florida Atlantic University are

> (1) to develop high-resolution methods for characterizing the spatial and temporal behavior of the normal mode field in shallow water; (2) to use this characterization as input data to inversion techniques for inferring the acoustic properties of the shallow-water waveguide; and (3) to use this characterization to improve our ability to localize and track sources. [1]

This thesis will focus on inversion techniques and inferring the properties of the seabed.

The objective of this research is to determine subbottom sound speed profiles for the significantly different environments observed in the SW06 experiment, termed “Channel” and “No Channel”. There are Compressed High Intensity Radar Pulse (CHIRP) and modal inversion results that accurately depict a “No Channel” region outside of the SW06 area of measurement that were used as a base model for these profiles [14]. Later models were based on CHIRP data within the region of the experiment.

1.2 Modal Mapping Experiment

The data this work is based on are from the Shallow Water ’06 (SW06) Modal Mapping Experiment (MOMAX). This experiment was conducted in the summer of 2006 at a location about 100 miles east of Atlantic City, New Jersey. This site has previously served as a natural laboratory for seabed studies in marine geology and has been shown to be characterized by a high degree of spatial variability of the sediment sound speed structure [2, 14, 33, 45]. The equipment consisted of four drifting MOMAX buoys named Moe, Larry, Shemp, and Curley, each with two hydrophones at depths of 40 m and 43 m and equipped with GPS; and a drifting source at a depth of 60 m that emitted tones of distinct frequencies: 50 Hz, 75 Hz, 125 Hz, and 175 Hz. Data were also received on a moored 8-channel Webb vertical line array and temperature measurements were obtained from the source string, the buoys, and the Webb vertical line array. A diagram of a MOMAX buoy is shown in figure 1.1 and a diagram of the experiment set up is shown in figure 1.2.

High resolution environmental data are required for accurate predictions of acoustic propagation and scattering in shallow water [21]. The area surrounding that of the SW06 experiment had been extensively surveyed in 2001-2002 using CHIRP sonar [2, 3] creating a grid of closely spaced tracks which provided knowledge of buried subbottom river channels. The buoys each spent time drifting over both channel and channel-free regions during the experiment. This CHIRP data provided the basis for a stratigraphic model for this area [4], shown in figure 1.3, as well as being used to create a complete three dimensional representation of the bottom inhomogeneities [33]. The paths the buoys took are shown in figure 1.4.

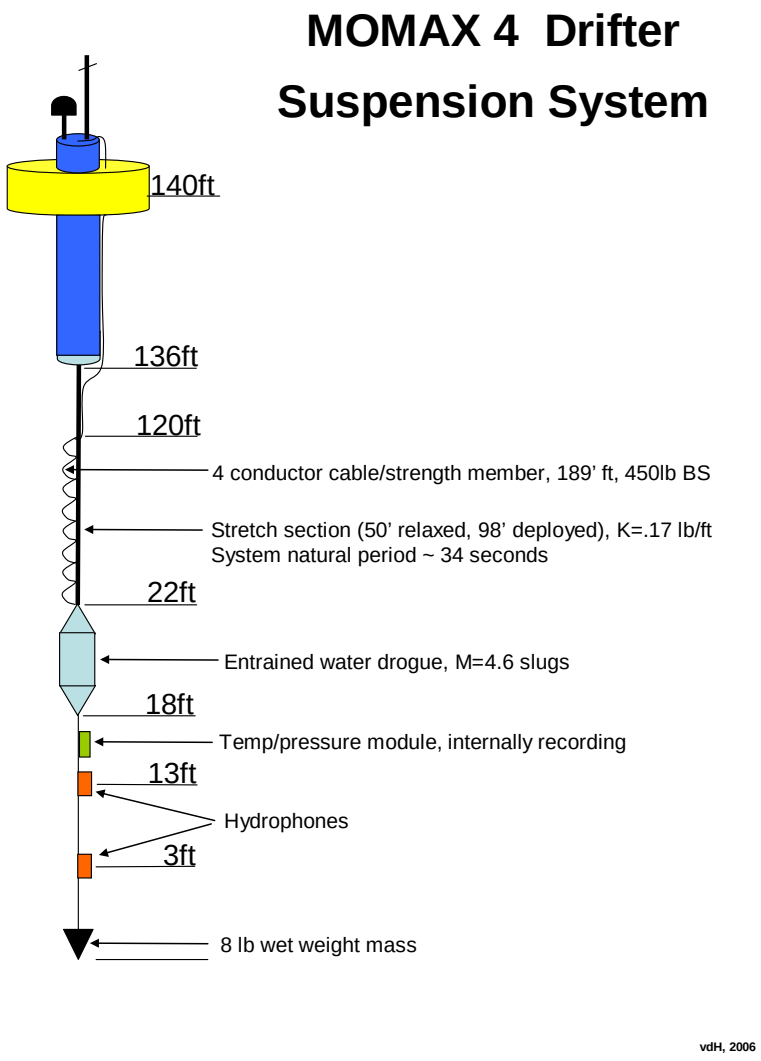

Figure 1.1: Diagram of the MOMAX buoy used in SW06

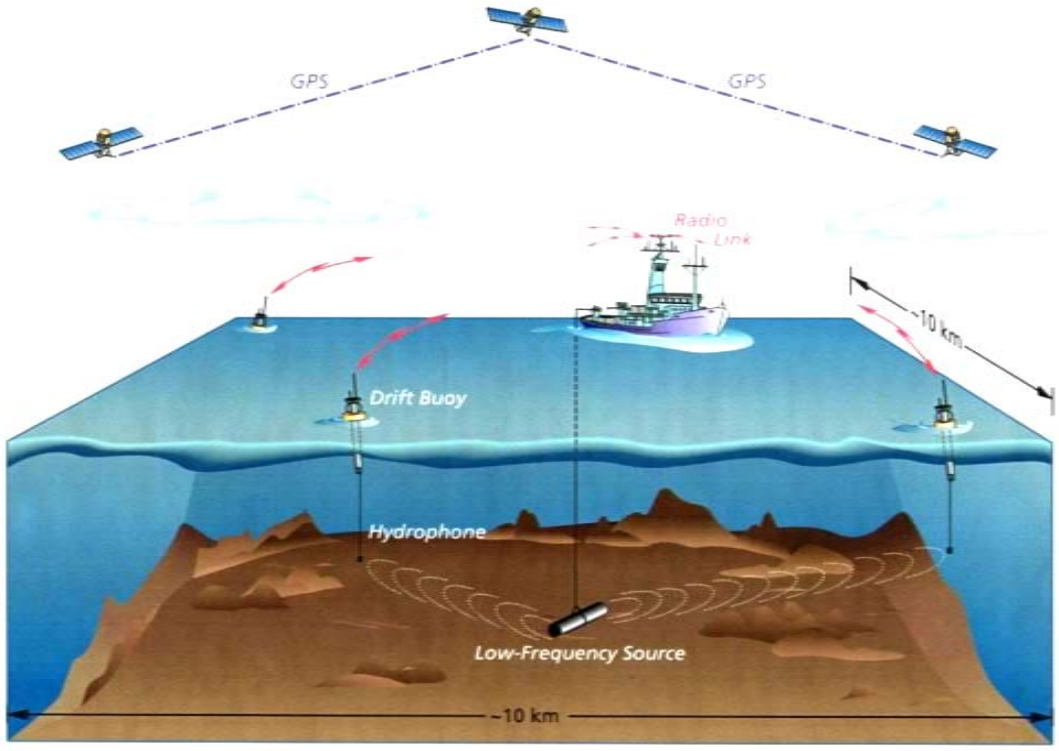

Figure 1.2: SW06 experiment set up

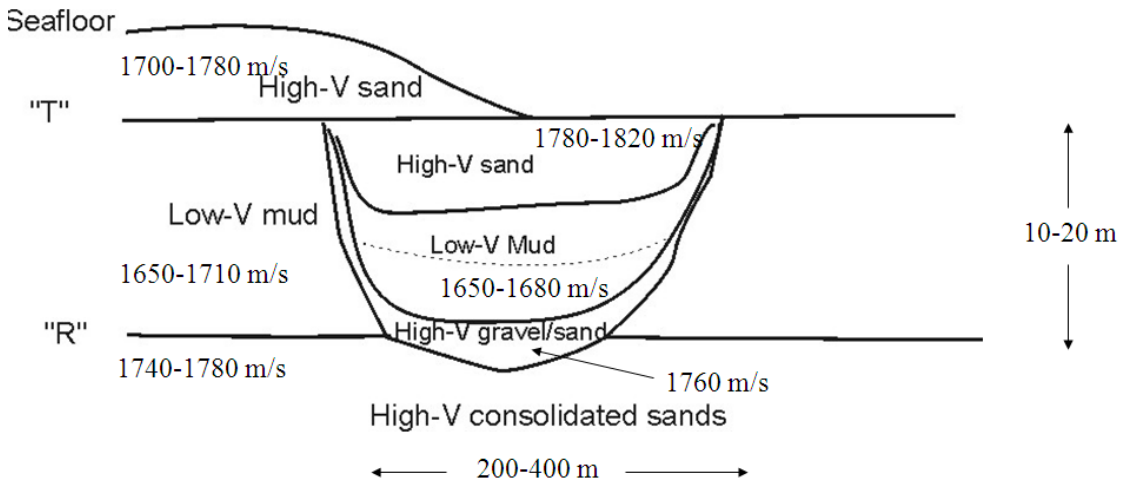

Figure 1.3: Stratigraphic model based on CHIRP data

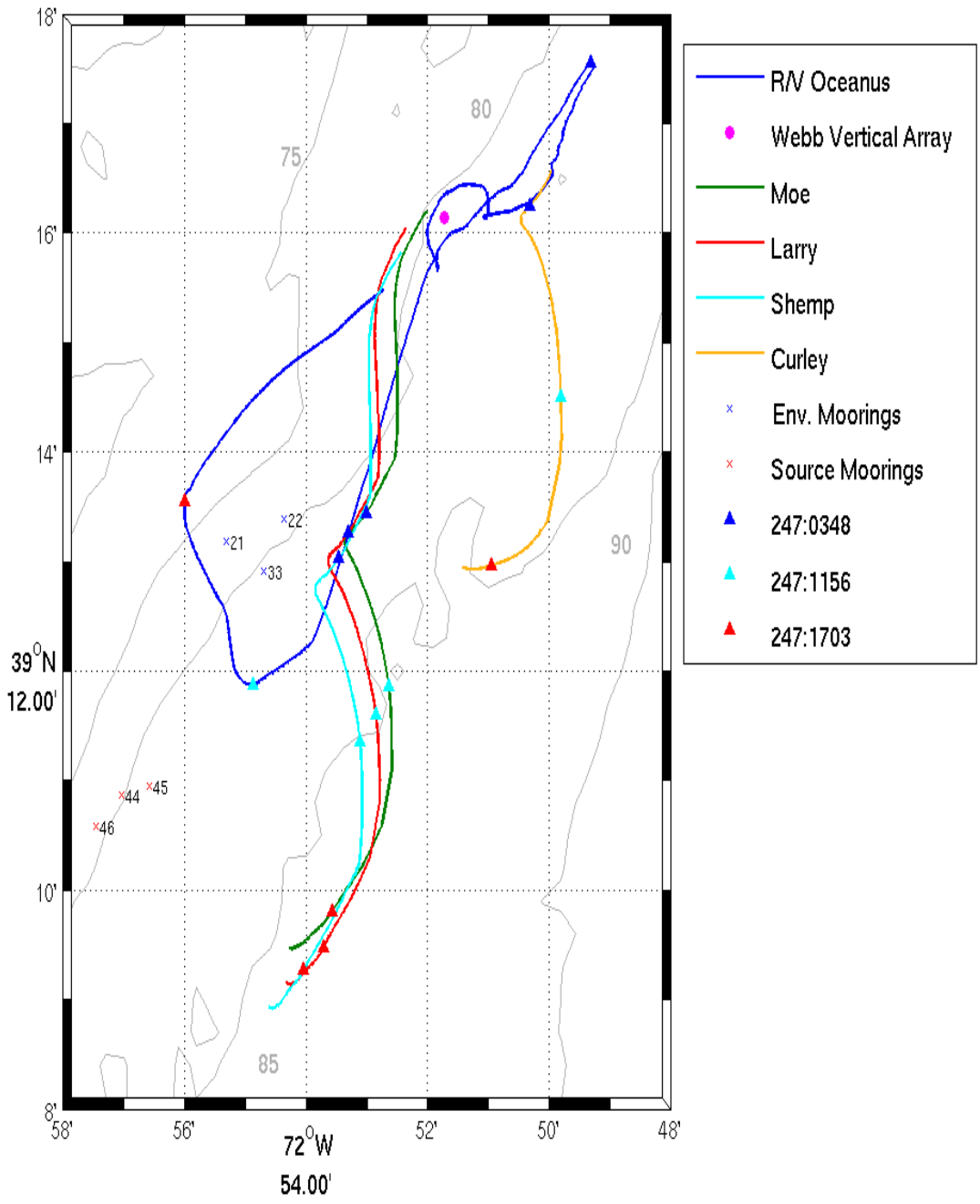

Figure 1.4: Paths of buoys, source, and environmental mooring locations

1.3 Background

1.3.1 Normal Mode Theory

In water less than 200 m in depth and with frequencies less than 500 Hz, the acoustic field can be described by a sum of normal modes that correspond to standing waves in depth and propagating waves in range [5, 6]. In the case these conditions are met, the method of normal modes is used to determine modal characteristics, which depend on the properties of the water column and its boundaries.

The method of normal modes is equivalent to the construction of the Green's function using an eigenfunction expansion [6]. The response of a wave-mechanical system to an arbitrary driving force can be expressed using these normal modes.

The inhomogeneous, time-independent wave equation in cylindrical coordinates, where **r**=(r,θ,z) and the wavenumber k(z)=ω/c(z), is (assume harmonic time dependence $e^{-i\omega t}$) [6]

$$\nabla^2 p(\boldsymbol{r}) + \rho(z)\nabla\left[\frac{1}{\rho(z)}\right]\cdot\nabla p(\boldsymbol{r}) + k^2(z)p(\boldsymbol{r}) = -4\pi\frac{\delta(r)}{r}\delta(\theta)\delta(z-z_0). \tag{1.1}$$

where $p(\boldsymbol{r})$ is the pressure field, $\rho(z)$ is the density, and z_0 is the source depth.

The complete solution to this wave equation is

$$p(r,z) = i\pi\sum_{n=1}^{\infty} a_n(z_0)p_n(r,z) = \frac{i\pi}{\rho(z_0)}\sum_{n=1}^{\infty} u_n^*(z_0)u_n(z)H_0^{(1)}(k_n r) \tag{1.2}$$

where the $p_n(r,z)$ are the normal modes of the waveguide, $u_n(z)$ is the eigenfunction, and $H_0^{(1)}(k_n r)$ is the zero-order Hankel function of the first kind:

$$p_n(r,z) = u_n(z)H_0^{(1)}(k_n r). \tag{1.3}$$

In the far field ($k_n r \gg 1$), Eq. 1.2 has the form

$$p(r,z) = A\sum_{n=1}^{\infty} u_n(z_0)u_n(z)\frac{e^{ik_n r}}{\sqrt{k_n r}}. \tag{1.4}$$

The vertical eigenfunctions $u_n(z)$ and the eigenvalues k_n satisfy the equation [6, 7]

$$\frac{d^2u_n(z)}{dz^2} + [k^2(z) - k_n^2]u_n(z) = 0. \tag{1.5}$$

Normal mode theory assumes variability in only one dimension (depth) when the more realistic case is in fact variability in three dimensions. An intermediate case in which the acoustic properties vary in two dimensions, range and depth, is the adiabatic mode theory in which the variation in range is much slower than the variation in depth. The inhomogeneous, time-independent wave equation where **r**=(r,θ,z) and the wavenumber k(r,z)=ω/c(r,z) is [6]

$$\nabla^2 p(\boldsymbol{r}) + \rho(r,z)\nabla\left[\frac{1}{\rho(r,z)}\right]\cdot\nabla p(\boldsymbol{r}) + k^2(r,z)p(\boldsymbol{r}) = -4\pi\frac{\delta(r)}{r}\delta(\theta)\delta(z-z_0), \tag{1.6}$$

and the complete solution to the wave equation is

$$p(r,z) \sim \frac{\sqrt{2\pi}e^{i\pi/4}}{\rho(0,z_0)}\sum_{n=1}^{\infty} u_n^*(0,z_0)u_n(r,z)\frac{\exp\left[i\int_0^r k_n(r)dr\right]}{\sqrt{k_n(r)r}}. \tag{1.7}$$

The eigenfunctions $u_n(r,z)$ and the eigenvalues $k_n(r)$ satisfy the local equation [6]

$$\frac{d^2u_n(r,z)}{dz^2} + [k^2(r,z) - k_n^2(r)]u_n(r,z) = 0 \tag{1.8}$$

As an example of the influence of the boundaries on the eigenvalues, consider the range-independent case of a homogeneous fluid layer bounded by horizontally stratified media with reflection coefficients R_s above and R_B below, shown in figure 1.5. A method for determining the characteristic equation for eigenvalues is described in Tolstoy and Clay [17] and Clay and Medwin [18].

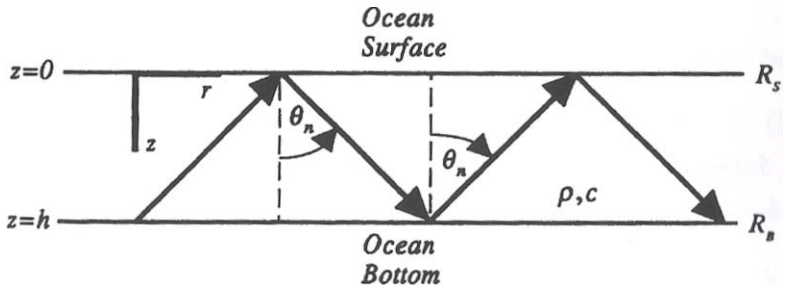

Figure 1.5: Homogeneous fluid layer bounded by horizontally stratified media with plane wave reflection coefficients R_s and R_B. [6]

The depth dependent $u(z)$ with no sources is a sum of up-going and down-going waves

$$u(z) = u_d(z) + u_u(z) = Ae^{ik_z z} + Be^{-ik_z z} \tag{1.9}$$

where A and B are constants determined by the boundary conditions.

At the surface,

$$R_s = \frac{u_d(z)}{u_u(z)}\bigg|_{z=0} = \frac{A}{B}, \tag{1.10}$$

and at the bottom,

$$R_B = \frac{u_u(z)}{u_d(z)}\bigg|_{z=h} = \frac{B}{A}e^{-2ik_z h}. \tag{1.11}$$

By combining (1.9) and (1.10), the following eigenvalue equation is obtained:

$$1 - R_s R_B e^{2ik_z h} = 0. \tag{1.12}$$

1.3.2 Perturbative Inversion

An inverse method is one that determines the properties of the media based on measurements of the acoustic field. There are many iterative methods available to determine bottom geoacoustic parameters [8-11, 15]. Specific feature methods invert the dominant feature to result in geoacoustic parameters, but can become ineffective if other effects interfere with the dominant feature. Iteration of forward models uses theoretical acoustic fields for various values of the bottom parameters until a best fit is found, but this method is time consuming and is not a true inverse method because only solutions to the forward problem are found. Perturbative inversion makes small perturbations around an assumed background model until a best fit is found for the input parameters. Exact inverse methods are non-perturbative and therefore do not require a background model, but are difficult to implement on real data [8].

The method used here is perturbative inversion, which is based on making small perturbations to a background model, c_b(z), using measured eigenvalues as the input data [10].

The wavenumber of the background is

$$k_b(z) = \frac{\omega}{c_b(z)}\,, \tag{1.13}$$

and the perturbed wavenumber is

$$k(z) = \omega/[c_b(z) + \Delta c(z)] \tag{1.14}$$

where $\Delta c(z)$ is the perturbation of the background model. The difference between the measured and background wavenumbers, $\Delta k_n = k_n - k_{bn}$, where k_n is the measured eigenvalue and k_{bn} is the background eigenvalue, for mode *n* is

$$\Delta k_n = \frac{1}{k_{bn}} \int_0^\infty \rho_b^{-1}(z) u_{bn}^2(z) k_b^2(z) \frac{\Delta c(z)}{c_b(z)} dz \tag{1.15}$$

where $u_{bn}(z)$ and $\rho_b(z)$ are the background mode function and density, respectively. This result shows that linear inverse theory can be applied to obtain $c(z)$.

The resulting eigenvalues are then compared to the measured input values, and the background is iterated until the eigenvalues resulting from the inversion agree with the input values [2, 9, 10, 11]. Iteration ends when the mismatch between the measured data and the data produced has been reduced to an acceptable level [45].

1.3.3 Wavenumber Estimation

The classical approach to spectral analysis to determine wavenumbers uses the Fast Fourier Transform with a Hann window applied to data from the full aperture [9]. Using this method, closely spaced wavenumbers cannot be resolved, and values will be inaccurate if the aperture contains a rapidly changing environment in range. An example of this full aperture spectrum is shown in figure 1.6. A high-resolution estimator is necessary to resolve closely spaced wavenumbers and to view the evolution of wavenumbers with range.

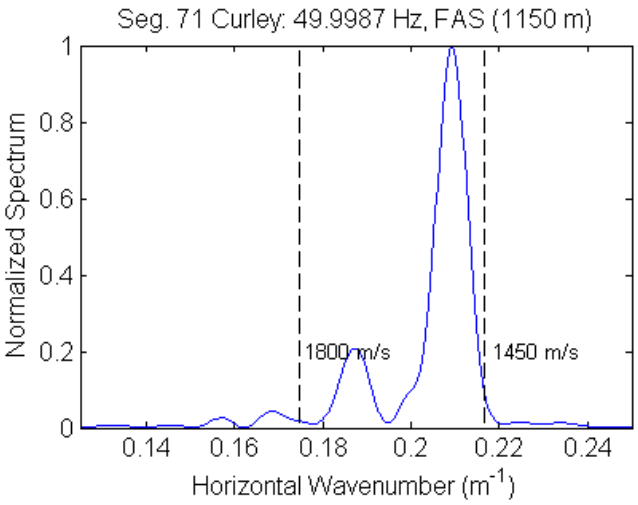

Figure 1.6: Full aperture spectrum wavenumber estimator

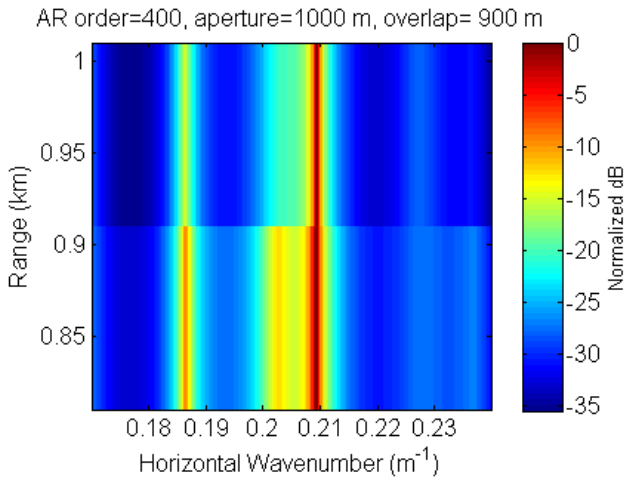

Figure 1.7: Autoregressive spectral estimator

The method used in this work for the estimation of modal eigenvalues is a sliding window autoregressive spectral estimator [9, 11]. This method was used because it does not require the large apertures to resolve low order modes that the short-time Fourier transform requires, and allows for the tracking of modal evolution with range [9, 11, 24], as shown in figure 1.7. This means this approach is useful in an environment that is rapidly changing. Eigenvalues are determined at each range step and depend on the local acoustic properties of the water column and seafloor. A range-dependent environment is approximated by a series of range-independent environments with a certain amount of overlap between the apertures in range. A high rate of overlap, 99%, was used in this work to aid in picking the peak locations from the spectrum in the midst of spurious peaks and peak broadening [24].

In this method, an estimator is used to find peaks in the depth-dependent Green's function that correspond to the horizontal wavenumbers of the propagating modes [9]. An autoregressive spectral method was chosen for its high-resolution frequency estimation property [12]. The theoretical resolution of AR based frequency estimation is [13]

$$\delta f = \frac{1.03}{Tp[SNR_{lin}(p+1)]^{0.31}} \tag{1.16}$$

where δf is the resolution, T is the sample interval in seconds, p is the AR order, and SNR_{lin} is the signal-to-noise ratio in linear units. As the SNR decreases, the advantage of using the AR estimator will also decrease [9].

The measured data can be related to the input data through a transfer function. The linear difference equation is

$$x_n = \sum_{l=0}^{q} b_l w_{n-l} - \sum_{k=1}^{p} a_k x_{n-k} \tag{1.17}$$

where w_n is the input driving sequence with parameters b_l, and x_n is the output sequence with parameters a_k. Their z-transforms are

$$A(z) = \sum_{m=0}^{p} a_m z^{-m}, \tag{1.18}$$

$$B(z) = \sum_{m=0}^{q} b_m z^{-m}, \tag{1.19}$$

and the transfer function is

$$H(z) = \frac{B(z)}{A(z)}. \tag{1.20}$$

The power spectrum of the output is

$$P_x(z) = H(z)H^*(1/z^*)P_n(z) = \frac{B(z)B^*(1/z^*)}{A(z)A^*(1/z^*)} P_n(z) \tag{1.21}$$

where $P_n(z)$is the power spectrum of the input.

The Autoregressive spectral estimator is an all-pole model of the transfer function, so the first term on the right hand side of the difference equation becomes $b_0 = 1$, therefore

$$x_n = -\sum_{k=1}^{p} a_k x_{n-k} + w_n \tag{1.22}$$

Evaluated along the circle $z = \exp(i2\pi fT)$ with variance σ^2 and written in terms of a_k, the power spectrum becomes

$$P_{AR} = \frac{\sigma^2 T}{\left|1 + \sum_{k=1}^{p} a_k \exp(-i2\pi fkT)\right|^2} \tag{1.23}$$

The AR parameters are a_k and σ^2, and peaks occur when the denominator is zero.

1.4 Outline of Work

Chapter 2 describes the Kraken Normal Mode program and its use to develop the original models of the sediment sound speed profiles. Kraken was used to determine if the assumed models could provide eigenvalues in the appropriate range compared with the measured values.

Chapter 3 describes the inversion program, which was the main source of data for this thesis. The inversion program uses the known eigenvalues from the buoy, Curley, as inputs and results in a sound speed profile using a perturbative method. This program was originally used with data from only one frequency at a time and was later used with data from multiple frequencies simultaneously.

Chapter 4 explains the importance of mode identification and how modal spectroscopy was used to accurately identify the modes at each frequency.

Chapter 5 examines the use of constraints during the inversion process so as to not allow sound speed values above or below certain points in order to keep the result within the limits of reality.

Chapter 6 describes the application of all of these techniques to the other three buoys involved in the experiment (Moe, Larry, and Shemp).

Chapter 7 concludes this thesis with a summary of the present work and suggestions for future efforts. Future work includes gathering new stratigraphy information, looking for patterns in the modal spectroscopy, and using the method of Qualitative Regularization.

2.0 Early Models Based on the Kraken Normal Mode Program

During the SW06 experiment, the buoys drifted over a system of sub-bottom channels assumed to have layers of sediment of slower sound speed than the basement sediment. To analyze the difference between these regions for when a buoy was over a channel and when it was not, the data were broken into segmental data (chunks) rather than looking at the full range of data all at once. The segments focused on for this research were from Curley, chunks 71 and 72, shown in figures 2.1 and 2.2. The paths start at the square and the circle for the source and receiver, respectively, and are opening in range.

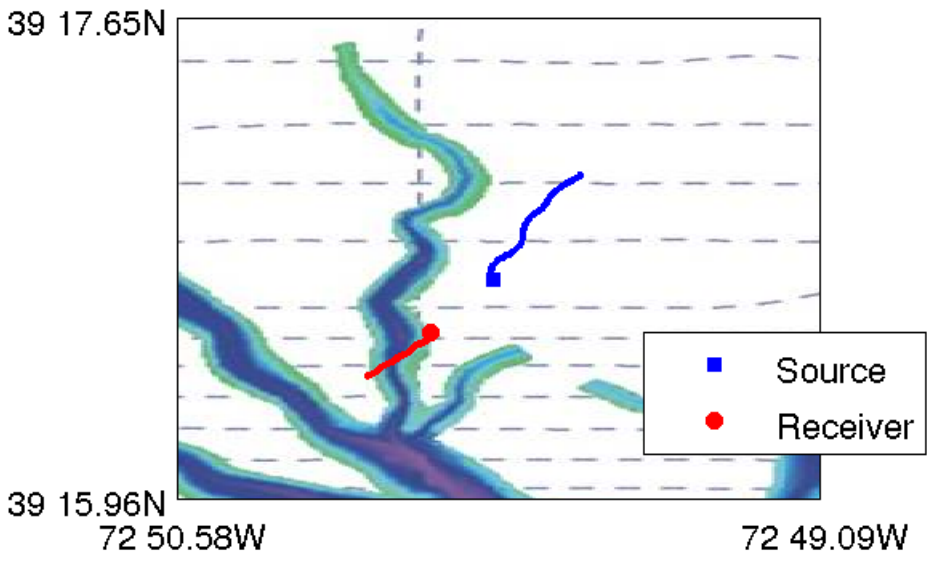

Figure 2.1: Curley Chunk 71, “Channel”

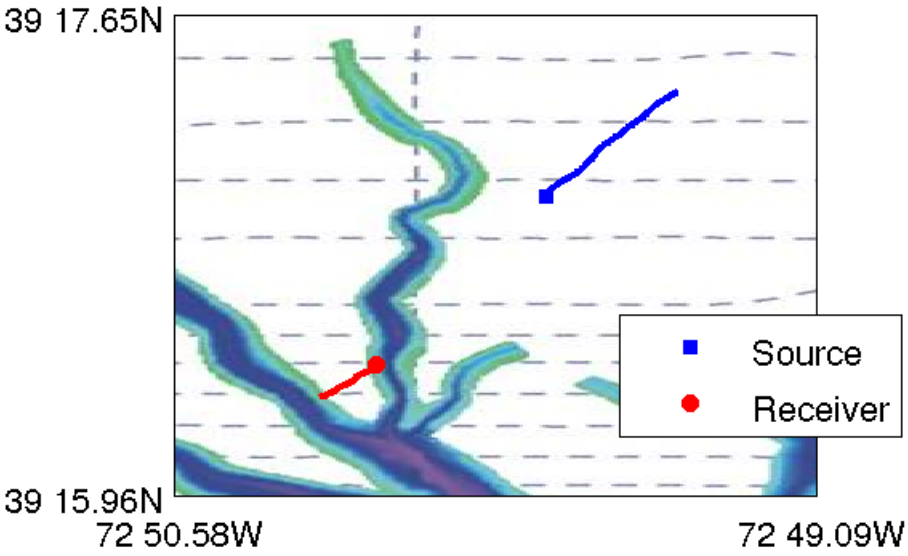

Figure 2.2: Curley Chunk 72, “No Channel”

Early models for these regions were based on CHIRP and modal inversion data (figures 2.3 and 2.4) from a region to the northeast of this experiment which was stratigraphically very similar to the “No Channel” section of data. The sound speed profiles of the models are shown in figure 2.5. The sound speed profile for the water column in these models was based on the average of the profiles taken over the course of the experiment.

KRAKEN is a program which computes the normal mode field for range-independent and range-dependent environments [19]. When using these profiles in the forward problem with the KRAKEN normal mode program, the resulting eigenvalues were almost exactly those from the pressure field obtained from the SW06 experiment.

Based on these pieces of background information along with the stratigraphic model, approximate depths of layers were assumed and sound speed profiles were developed to determine, using KRAKEN, if eigenvalues similar to the actual data could be simulated.

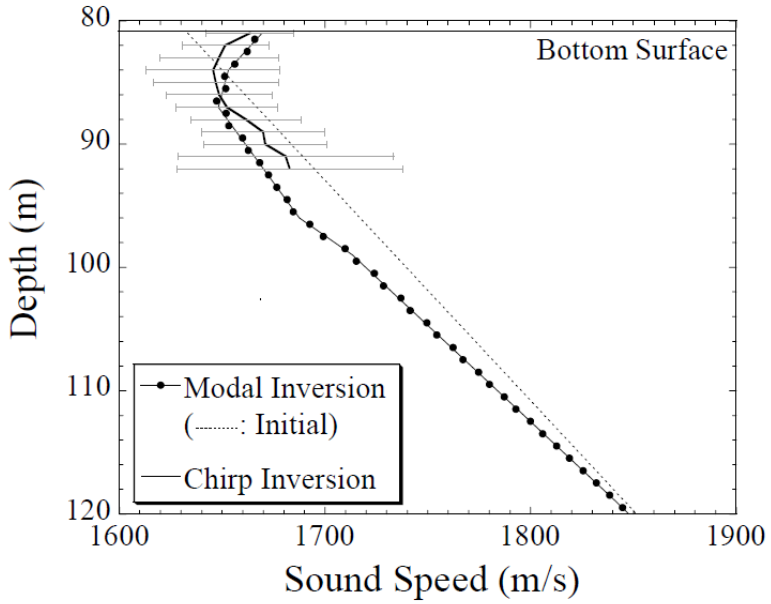

Figure 2.3: CHIRP and modal inversion results, [14]

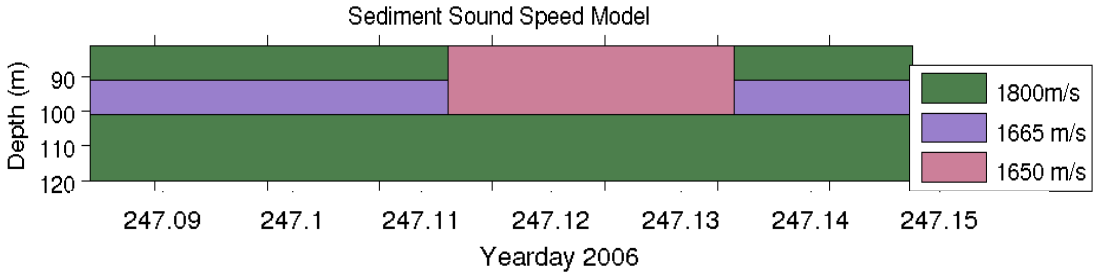

Channel No Channel Channel

Figure 2.4: Approximate depth of layers

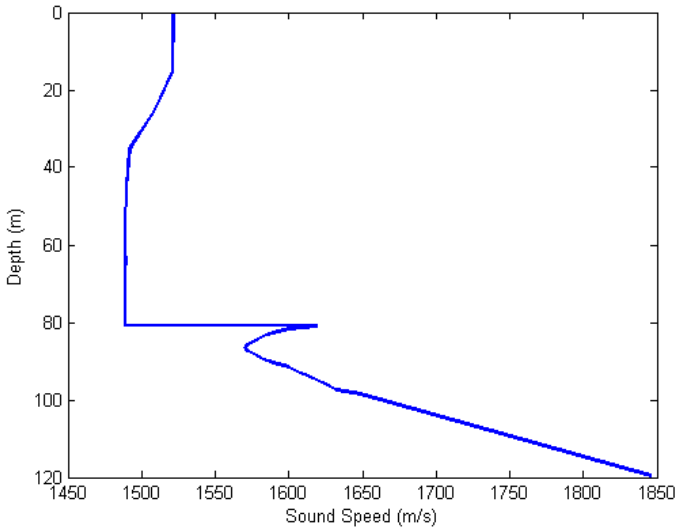

(a)

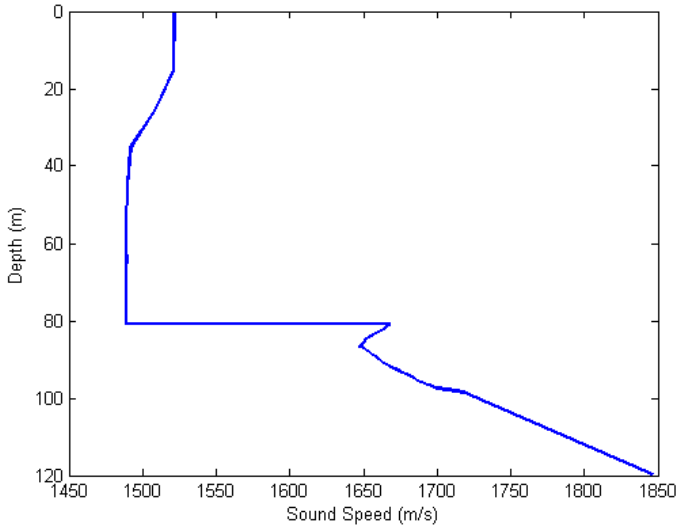

(b)

Figure 2.5: (a)Early model of “Channel” sound speed profile,
(b) Early model of “No Channel” sound speed profile

The eigenvalues from the data that these models were aiming for are listed in Table 2.1.

	Channel	**No Channel**	**Channel**
Mode 1	**0.209005**	**0.207854**	**0.208622**
Mode 2	**_**	**0.198263**	**_**
Mode 3	**0.186765**	**0.184836**	**0.186800**

Table 2.1: Eigenvalues obtained from the pressure field of the SW06 data

The simulated eigenvalues obtained through KRAKEN using these models were very close to the actual data as seen in figure 2.6.

This did show, however, that the second mode in the actual data seems to disappear while the buoy is over a channel. The observed disappearance of the mode may be due to the measurement being taken at a receiver depth near the node of the second mode [14].

An example of the data output of a single chunk of data is shown in figure 2.7. This includes the magnitude and phase of the pressure field, the map of the chunk, the full aperture spectrum of wavenumber, and the AR spectrum.

A map of the entire SW06 experiment showing where the channels are compared to the paths of the buoys can be seen in figure 2.8. The box indicates where these Curley chunks were compared to the other buoys.

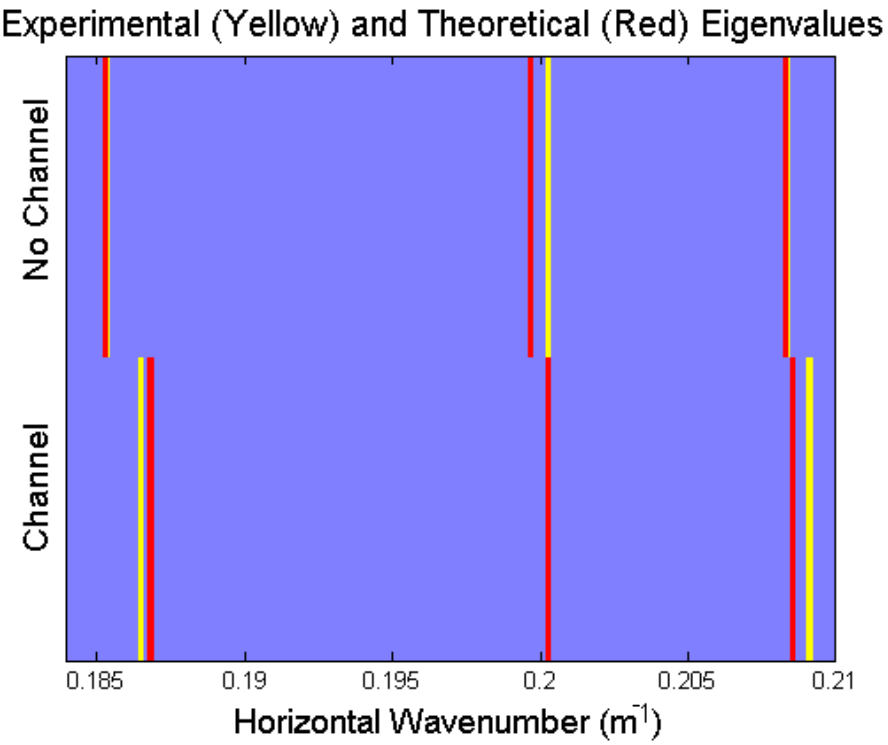

Figure 2.6: Eigenvalues from data (yellow) compared to theoretical (red)

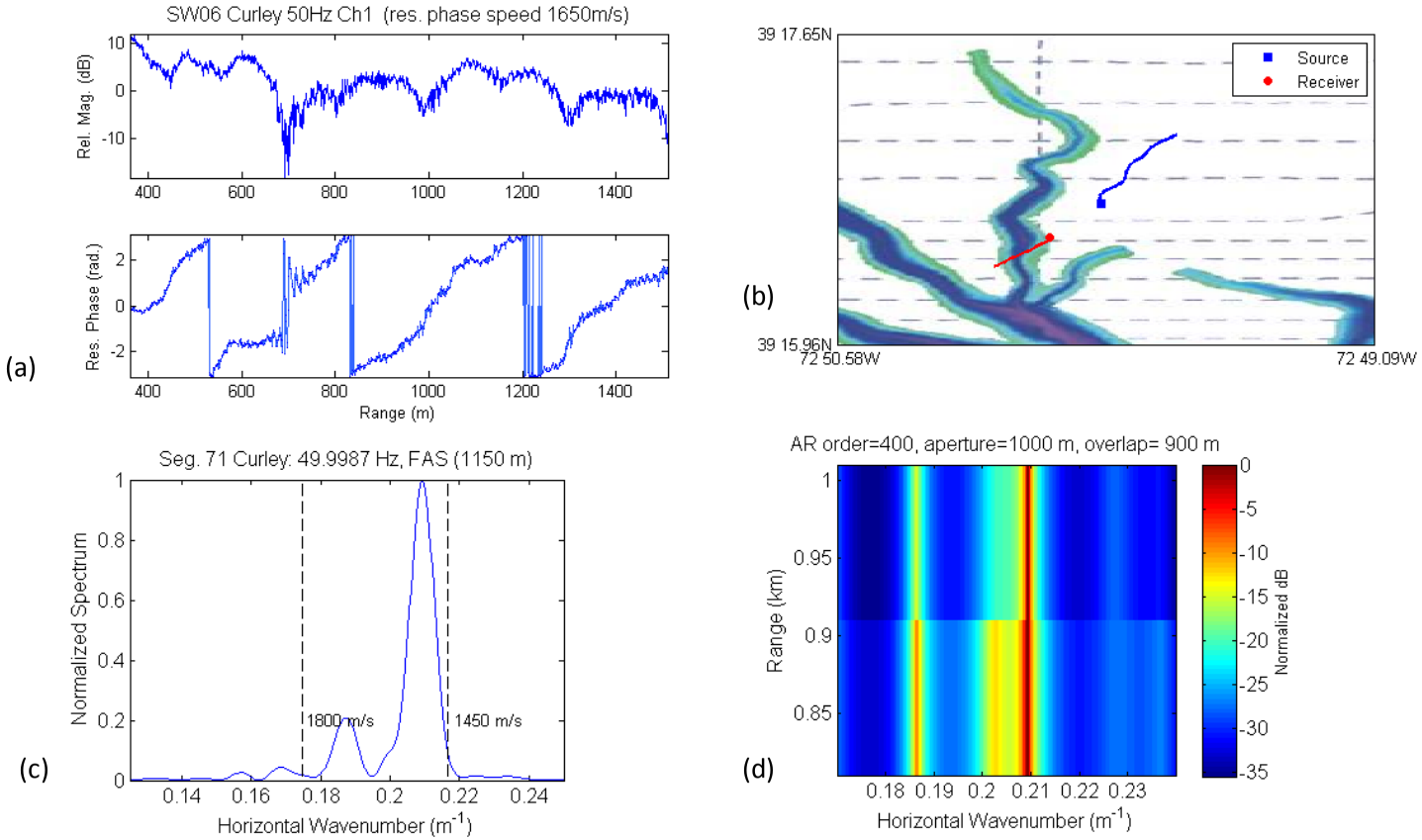

Figure 2.7: Data output of a single chunk. (a) pressure magnitude and phase, (b) map of chunk, (c) full aperture spectrum of wavemumber, (d) autoregressive spectrum.

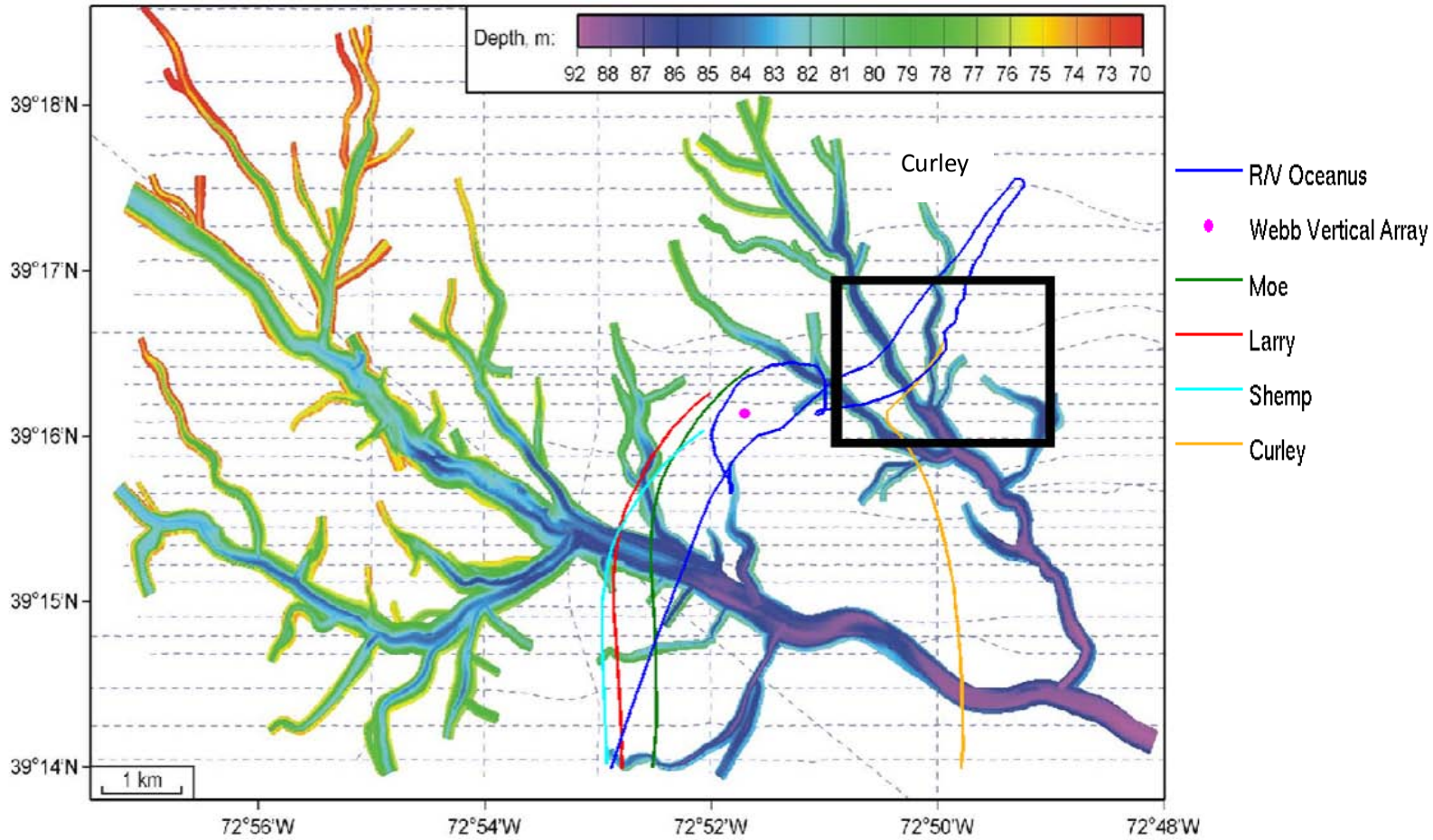

Figure 2.8: Paths of buoys with a map of the channels

3.0 Inversion Program

The process described in the previous section is the forward problem, which helped to determine that the proposed models do result in eigenvalues similar to those from the actual data. The next step is to use the eigenvalues from the actual data as the inputs into the inverse problem to determine the sound speed profiles for the environments using the proposed models as the basis for a "correct" inversion. This technique is appropriate for the highly variable shallow water environment because eigenvalues can be measured locally and their values are a direct measurement of the local environmental parameters [23, 24, 25].

A Matlab program [11] was used in which a single layer of a background profile is perturbed, so to perturb for the entire sediment as a whole the sediment must consist of a linear gradient overlaying a halfspace in the background. The sound speed profile of this background is shown in figure 3.1. Each iteration of this program results in a sound speed profile for which the eigenvalues are calculated and compared to measured eigenvalues that were given as inputs, and the differences between them are recorded. Another iteration will follow using the same steps in order to correct the eigenvalues that were not close enough to the measured, but this time the two sets of differences will also be compared. The iterations will continue until there is no noticeable variation in the differences from one iteration to the next. If the mean squared difference of the

perturbation values at each depth, $\Delta c(z_i)$, found using eq. 1.15, is less than one, then the inversion is complete:

$$\frac{1}{n}\sum_{i=1}^{n}(\Delta c(z_i))^2 < 1\,. \tag{3.1}$$

Other inputs include the frequency at which the measured eigenvalues are obtained and the number of iterations to run. The method of inversion used for this data set was Singular Value Decomposition (SVD) because it can be effectively applied to both under determined and over determined problems [15]. A detailed description of SVD can be found in Rajan, et al. [15].

The background model used for these inversions was a simple linear profile with the speed at the water/bottom interface set as 1800 m/s and the speed of the halfspace set at 1850 m/s. The assumed profile that these perturbations were aiming for was based on CHIRP data from a grid of closely spaced tracks over this region [4]. These data were provided as a function of two-way travel time arranged in layers which included assumed sound speeds and sediment material, and can be seen in figures 3.2 and 3.3 [16]. The second plot was needed because the first cut off the full length of the first channel. These channel structures were converted to a function of depth rather than travel time by treating each of the layers as isovelocity to approximate a depth. This depth plot can be seen in figure 3.4.

Inversions were carried out by using actual data from one frequency at a time and using eigenvalues from Receiver 1 at a depth of 40 m using an aperture of 700 m, shown in figures 3.5 and 3.6. All of the eigenvalues obtained can be seen in Table 3.1, but not all

of these were used. The eigenvalues too far above or below the expected values based on the Kraken results were excluded from the inversion data, and the eigenvalues that are shown in bold in Table 3.1 are the ones used.

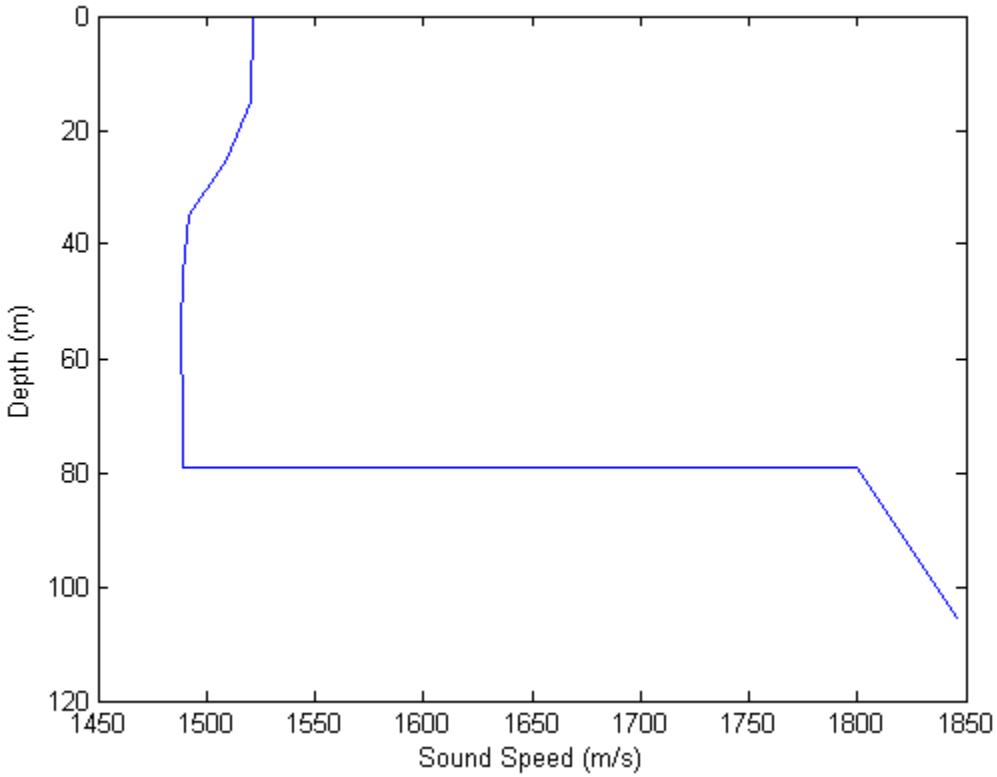

Figure 3.1: Background profile used in inversions

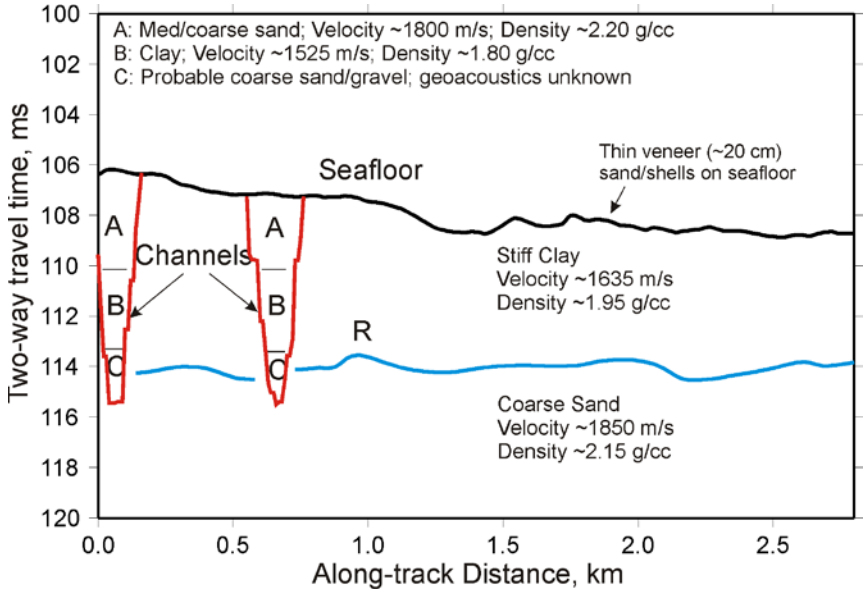

Figure 3.2: Channel structure vs. two-way travel time [16]

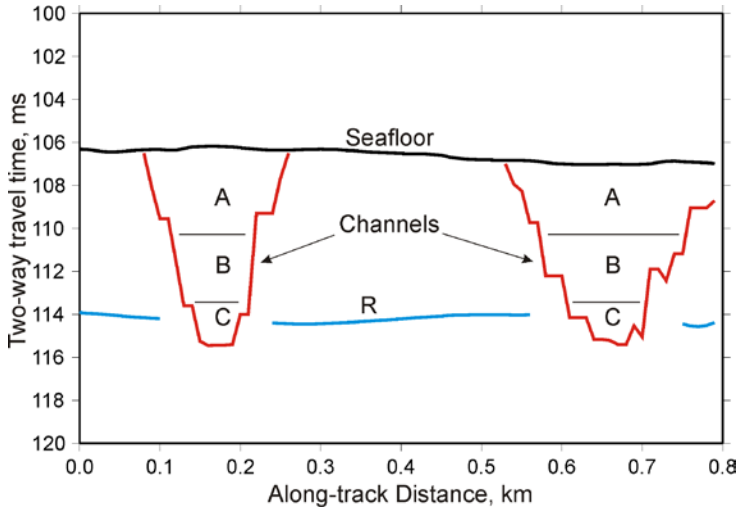

Figure 3.3: Channel structure vs. two-way travel time [16]

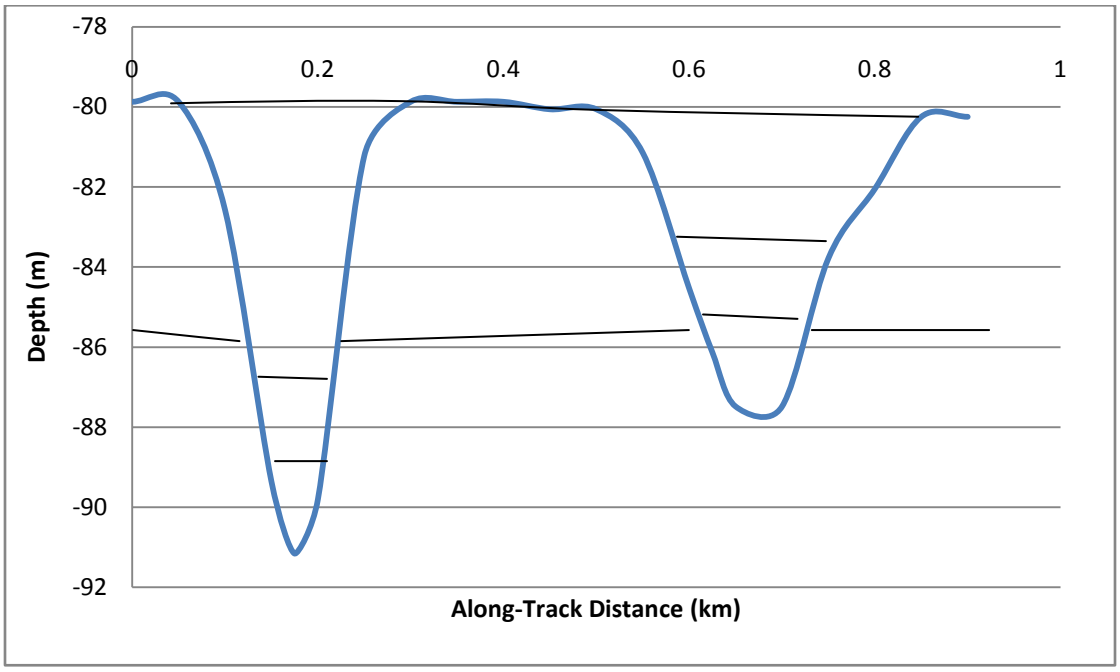

Figure 3.4: Channel structures vs. depth, assuming sound velocities shown in Fig. 3.2

Aperture: 700m Receiver 1

Channel

frequency	eigs							
50	0.236185	**0.210347**	**0.188847**	0.166628	0.139412			
75	**0.317965**	**0.305166**	**0.284577**	**0.262622**				
125	**0.529439**	**0.508658**	**0.481717**	**0.445142**				
175	0.797825	0.765672	**0.732487**	**0.720012**	**0.696199**	**0.672374**	**0.648370**	**0.611674**

No Channel

frequency	eigs					
50	**0.208273**	**0.191076**	0.163548			
75	**0.316012**	**0.284841**				
125	0.547882	**0.525412**	**0.503289**	**0.481682**	**0.449432**	
175	0.779082	**0.738587**	**0.717747**	**0.674711**	**0.645997**	**0.613136**

Table 3.1: Eigenvalues organized by frequency

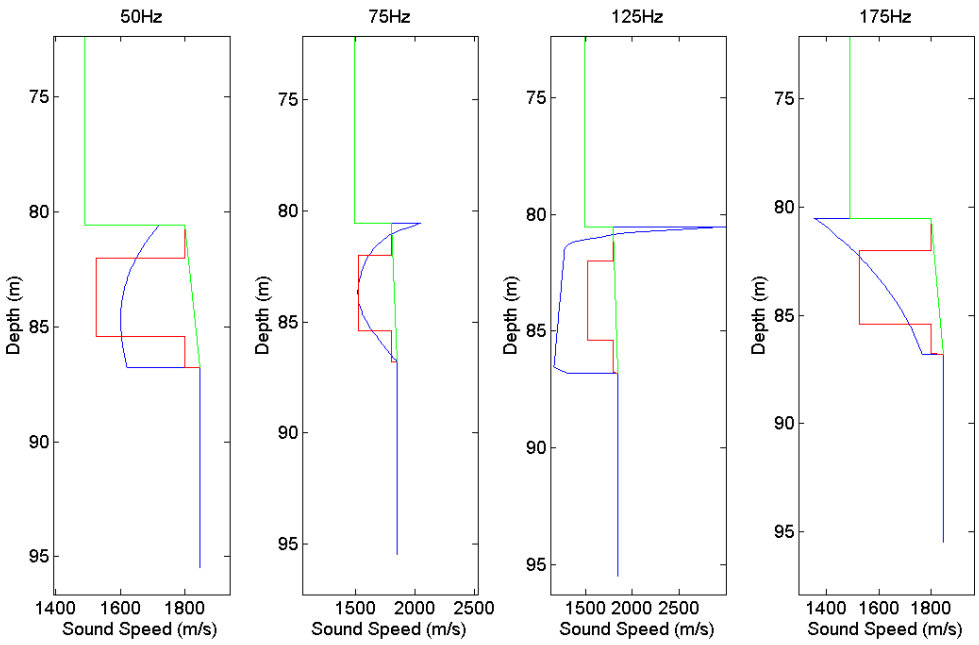

Figure 3.5: “Channel” Inversions by frequency; green is the background, red is the assumed, and blue is the inversion

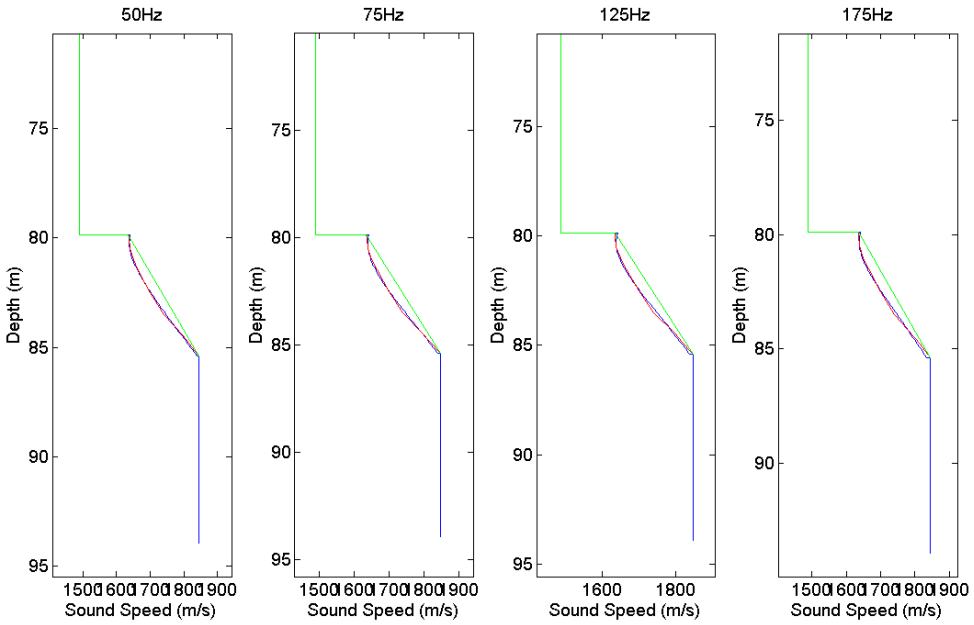

Figure 3.6: “No Channel” Inversions by frequency; green is the background, red is the assumed, and blue is the inversion

The inversions of the “channel” region vary greatly between each of the frequencies, whereas the inversions of the “no channel” region are very consistent. This shows that, while an accurate inversion of the stable “no channel” region should be rather straight forward, an inversion of the variable “no channel” region is more challenging and will need to be examined more closely.

3.1 Inversion Using Multiple Frequency Inputs

In order to improve the resulting sound speed profiles, data from multiple frequencies were used simultaneously in the inversion program, which resulted in profiles closer to the assumed result, shown in figure 3.7, in which the red profile is the assumed profile based on the stratigraphy and the blue is the inversion. Lower frequencies produce modes which penetrate significantly deeper into the sediment and higher frequencies make it possible to resolve smaller features because shorter wavelengths are more sensitive to detailed structure [45]. So, with more information used as inputs into the inversion program, the program was able to determine profiles with a higher chance of being accurate [11]. The mean squared difference between the measured and perturbed eigenvalues for these multiple frequency inversions for each iteration can be seen in figures 3.8 and 3.9. It can be seen that the “No Channel” inversion converged quickly, only requiring four iterations because the mean squared difference dropped off steeply after the first iteration and found the minimum. The “Channel” inversion required more iterations to find the minimum and did not converge as quickly.

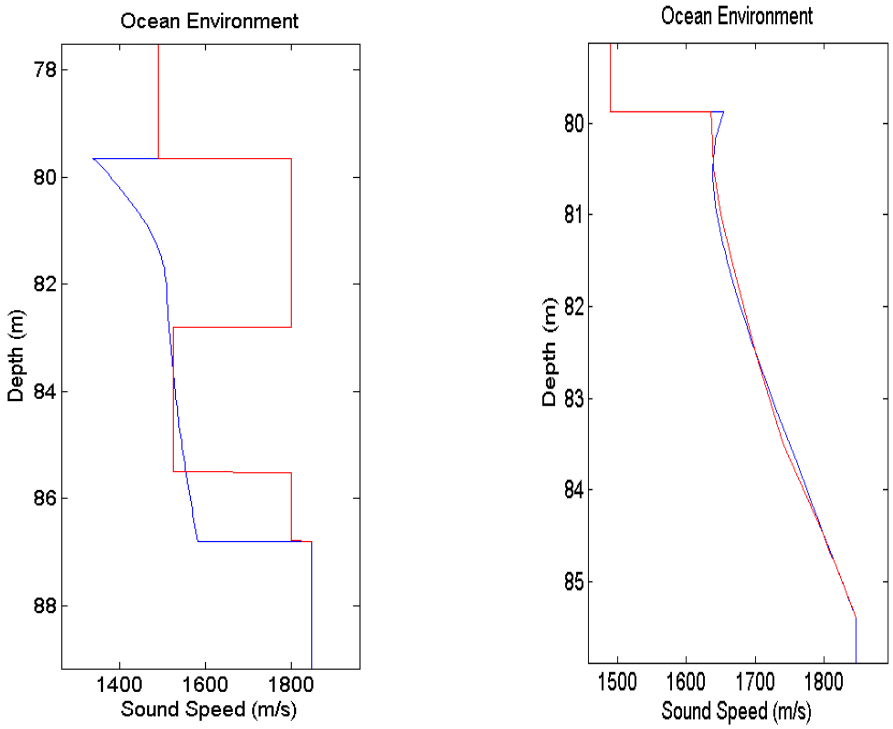

(a) **(b)**

Figure 3.7: Multiple frequency inversions (blue) and the assumed profile (red); (a) "Channel", (b) "No Channel"

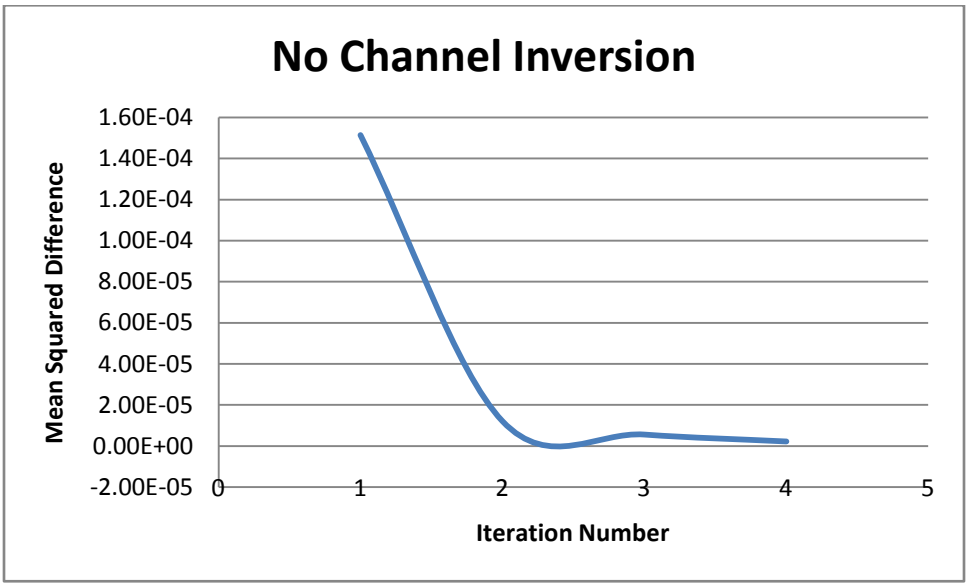

Figure 3.8: Mean Squared Error of Δk_n vs. iteration number for the "No Channel" inversion.

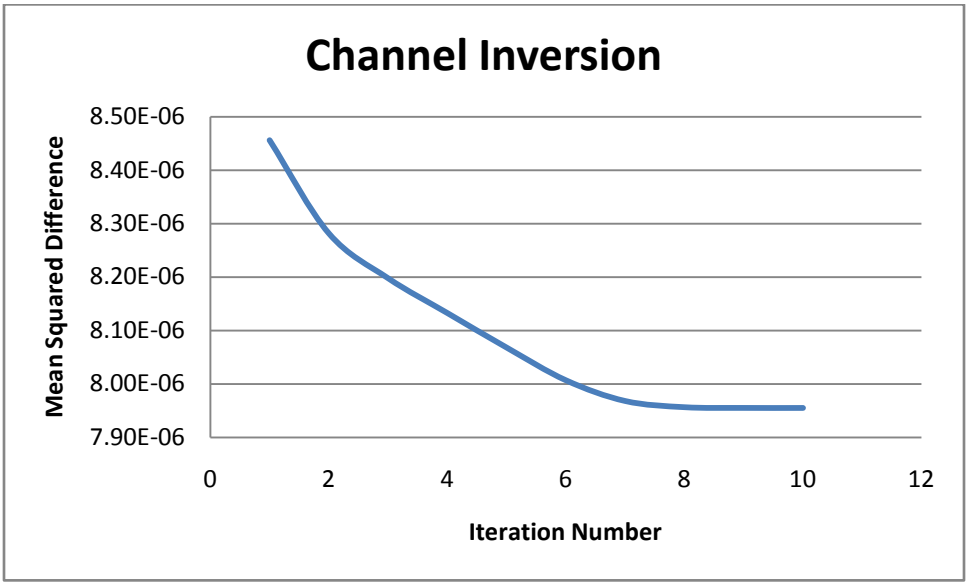

Figure 3.9: Mean Squared Error of Δk_n vs. iteration number for the "Channel" inversion.

4.0 Modal Spectroscopy

At first, the eigenvalues were entered into the inversion program in the order they appeared from the AR data; however, mode identification is very important. Since it was noticed in the very early models that the second mode seemed to disappear, it was possible that more modes disappeared. New plots were made to visually determine which eigenvalues should be paired between the “Channel” and “No Channel” regions. These were then compared with the simulated eigenvalues from KRAKEN to determine if a mode was not being represented in the actual data. In this inversion program, a mode can be identified while not knowing the exact eigenvalue by inserting a zero into its place. This method also helped to determine spurious peaks on either end of the data due to analysis error. The modal spectroscopy can be seen in figure 4.1.

4.1 Mode Identification

The number of modes propagating in a given waveguide, n_{max}, can be estimated as [6, 45]

$$n_{max} < \frac{2D}{\lambda}\sqrt{1-\frac{{c_w}^2}{{c_b}^2}}+\frac{1}{2} \tag{4.1}$$

where D is the depth of the waveguide, λ is the frequency, c_w is the speed of sound in the water, and c_b is the approximate speed of sound in the bottom. These values agree with the number of modes produced for each frequency using the Kraken models.

Using the modal spectroscopy, the eigenvalues from both receivers were identified as the mode number of the identified Kraken mode each was closest to. Any eigenvalues outside the range of the Kraken eigenvalues were considered spurious peaks in the AR and were not included in the inversion input data. Where there was a Kraken value but no matching measured value, it was assumed that this peak was not strong enough to see and was considered missing. A zero was used as a placeholder for these values in the inversion input data so the modes could be identified correctly.

Table 4.1 shows these eigenvalues organized by modal identification and by frequency. In this table, wherever there is a Kraken value and no receiver values, the zero placeholder was used. Wherever there is a receiver value and no Kraken value, this was considered spurious and was not used.

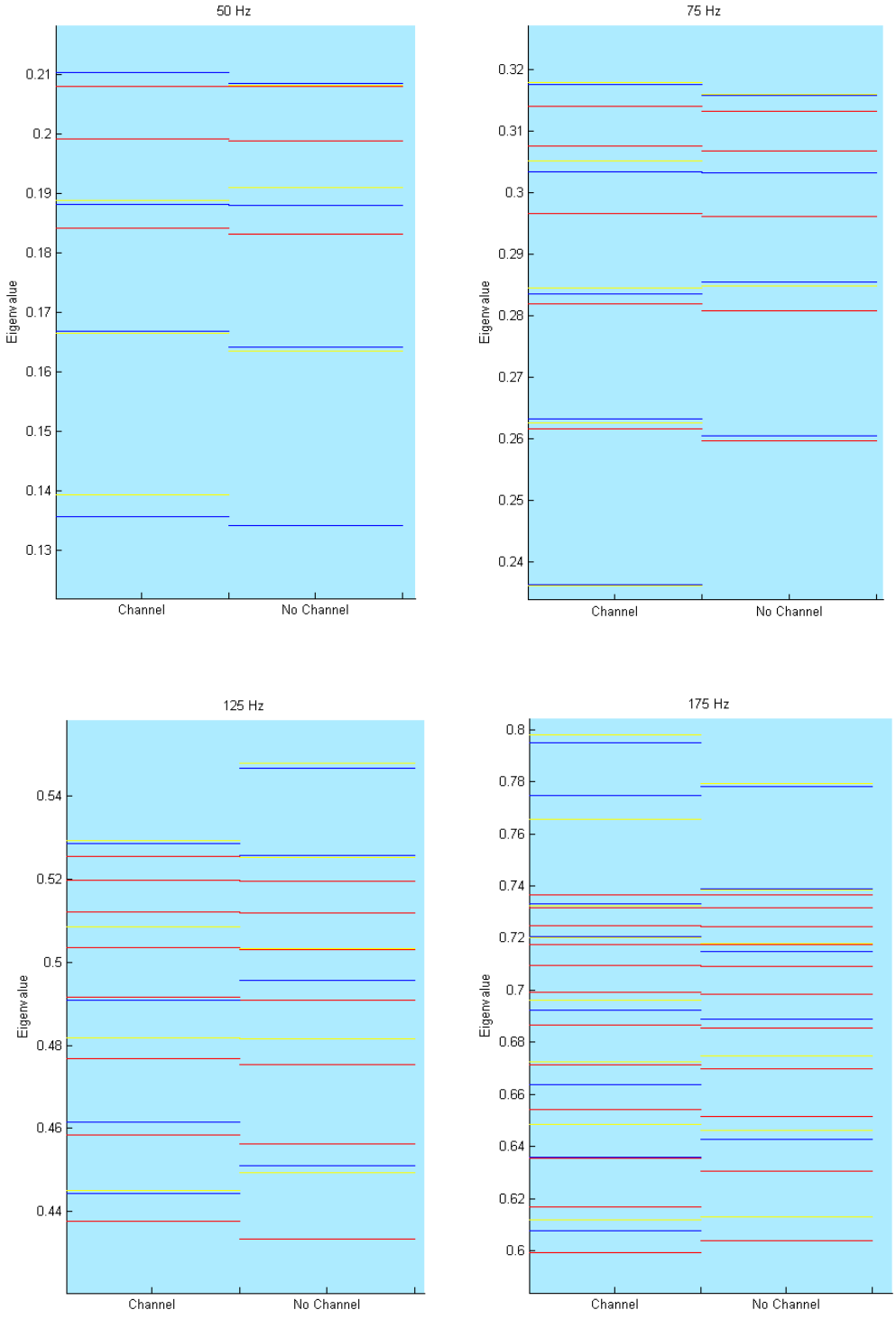

Figure 4.1: Modal Spectroscopy at each frequency; red for theoretical, yellow for Receiver 1, blue for Receiver 2

50 Hz								
Channel								
	Receiver 1	0.2361851	0.2103471		0.1888474	0.1666287	0.1394125	
	Receiver 2	0.2363049	0.2103591		0.1882362	0.1668324	0.1357693	
	Kraken		0.2081167	0.19924856	0.18417345			
No Channel								
	Receiver 1		0.2082738		0.1910765	0.1635487		
	Receiver 2		0.2085015		0.1879846	0.1642558	0.1342713	
	Kraken		0.2079857	0.1988399	0.18331049			

75 Hz							
Channel							
	Receiver 1	0.3179655	0.3051663		0.2845774	0.2626223	
	Receiver 2	0.3176539	0.3034885		0.2836067	0.2632575	
	Kraken	0.3140339	0.3076782	0.29671258	0.28191694	0.26163779	
No Channel							
	Receiver 1	0.3160120			0.2848411		
	Receiver 2	0.3157843	0.3033087		0.2854882	0.2605610	
	Kraken	0.3133415	0.3067678	0.2961485	0.28085373	0.25967227	

125 Hz											
Channel											
	Receiver 1		0.5294391		0.5086584			0.4817179		0.4451420	
	Receiver 2		0.5285523				0.4910296		0.4615485	0.4444350	
	Kraken		0.5254476	0.51975613	0.5122478	0.503567	0.49173095	0.47675166	0.45852345	0.43768699	
No Channel											
	Receiver 1	0.5478828	0.5254124			0.5032895		0.4816820	0.4494324		
	Receiver 2	0.5467563	0.5257479				0.4957634		0.4510862		
	Kraken		0.5253927	0.51957286	0.5119469	0.50306965	0.49086829	0.4753671	0.45621744	0.43345189	

175 Hz													
Channel													
	Receiver 1		0.7324878		0.7200122		0.6961996		0.6723749	0.6483705		0.6116748	
	Receiver 2		0.7331469		0.7205755			0.6924605	0.6637703		0.6359788		0.6075163
	Kraken	0.7367209	0.7316719	0.72473992	0.71767197	0.70960937	0.69914405	0.68645274	0.67135815	0.65420512	0.63542376	0.61697795	0.5991577
No Channel													
	Receiver 1	0.7385878			0.7177472				0.6747119	0.6459977		0.6131369	
	Receiver 2	0.7390072			0.7149669			0.6889731		0.6426660			
	Kraken	0.7366931	0.7315638	0.72453415	0.71740921	0.70915408	0.69842874	0.68533402	0.66965397	0.65148878	0.63062894	0.60376779	

Table 4.1: Eigenvalues organized by modal identification

5.0 Using Limits

The inversions resulted in profiles for the “channel” segment that were somewhat unrealistic; they showed speeds in the bottom that were significantly slower than the sound speed in the water. To see if the inversions could be pushed in the right direction, limits were implemented in the program such that the first time the profile had a value of less than 1000 m/s that point would be given the value of 1700 m/s and the program would continue inverting using that new point. Many combinations of limits were used to determine the best fit for what was assumed to be the actual profile based on the CHIRP data for the region, but the best fit was determined to be when the constraints were set to 1000 m/s and 1780 m/s. The inversion constrained to a set of limits can be seen in figure 5.1.

Although using limits resulted in more accurate profiles visually, it seemed that these inversions included too much manipulation to be truly accurate. To determine the validity of using limits, the mean squared error of the difference between the eigenvalues from the inverted profile using limits and the actual values was compared with the mean squared error from the profiles with no limits. The errors using the limits were on par with the errors without the limits, which can be seen in Table 5.1. The magnitude of the pressure fields of the inverted profiles were compared with the magnitude of the pressure field of actual data as another way to determine how accurate these inversions using limits were. The comparisons of the pressure fields can be seen in figures 5.2-5.

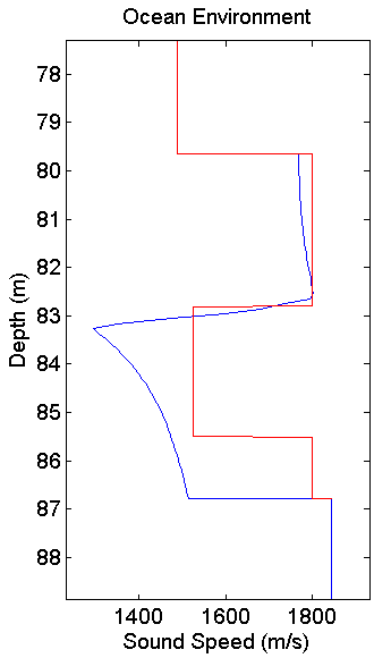

Figure 5.1: Inversion using multiple frequencies and limits

no limits	**limits**
0.0014	0.0021
-0.0056	-0.0041
-0.0042	-0.0021
0.0025	0.0045
0.000655	-0.0016
-0.0004	0.00005
0.0037	0.0048
-0.0023	-0.001
0.000872	0.0012
0.0033	0.0041
mean square difference	
0.000088	0.0000907

Table 5.1: Differences between calculated eigenvalues and measured eigenvalues with and without limits

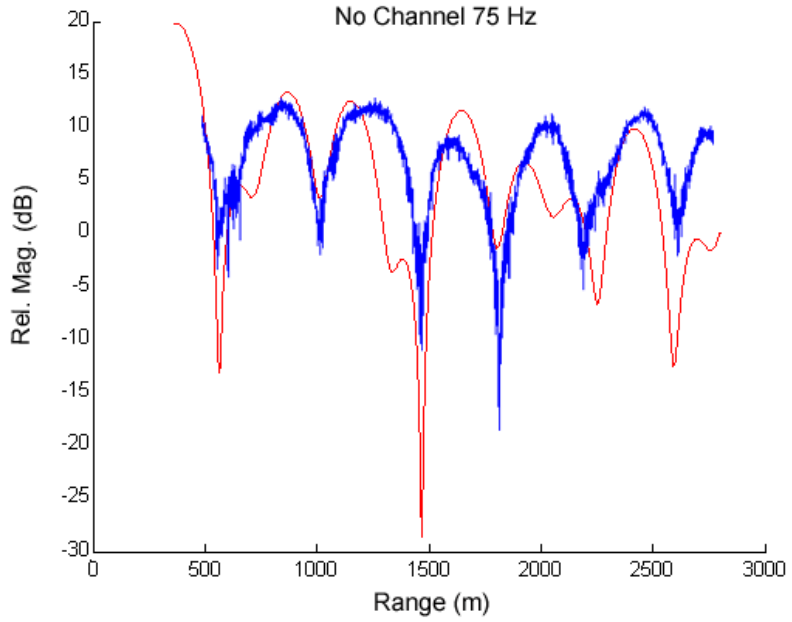

Figure 5.2: Comparison of pressure field magnitude from the inversion (red) and the data (blue) of Curley's 75 Hz No Channel

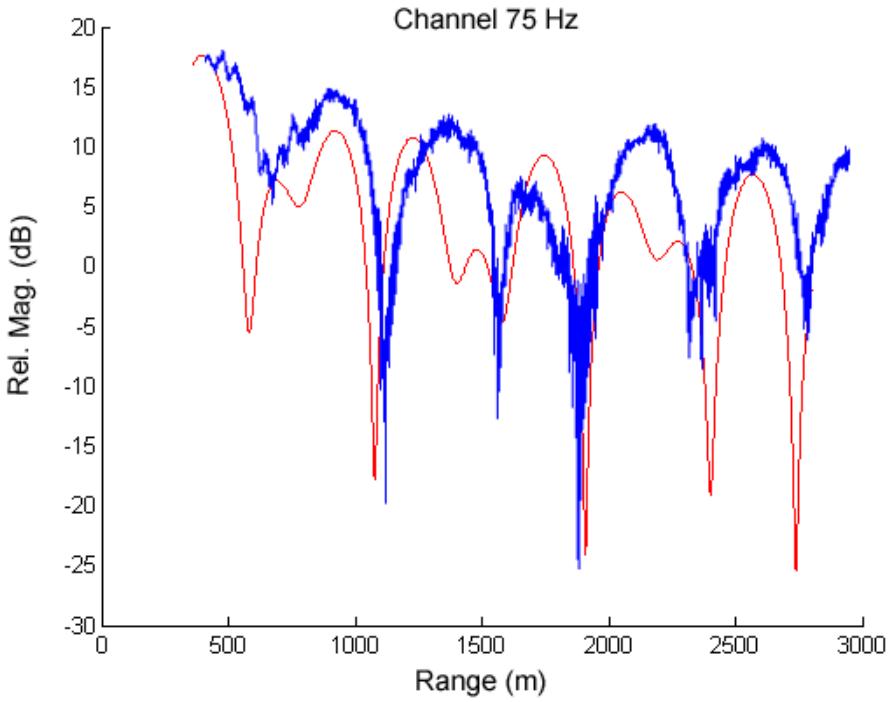

Figure 5.3: Comparison of pressure field magnitude from the inversion (red) and the data (blue) of Curley's 75 Hz Channel

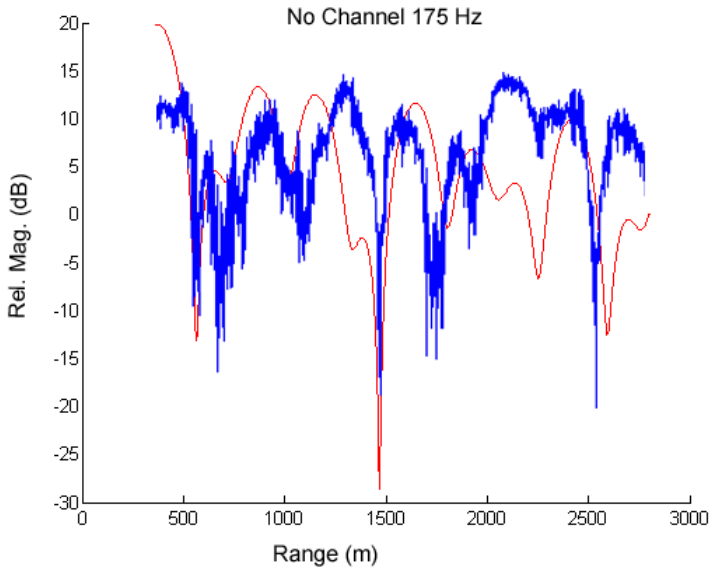

Figure 5.4: Comparison of pressure field magnitude from the inversion (red) and the data (blue) of Curley's 175 Hz No Channel

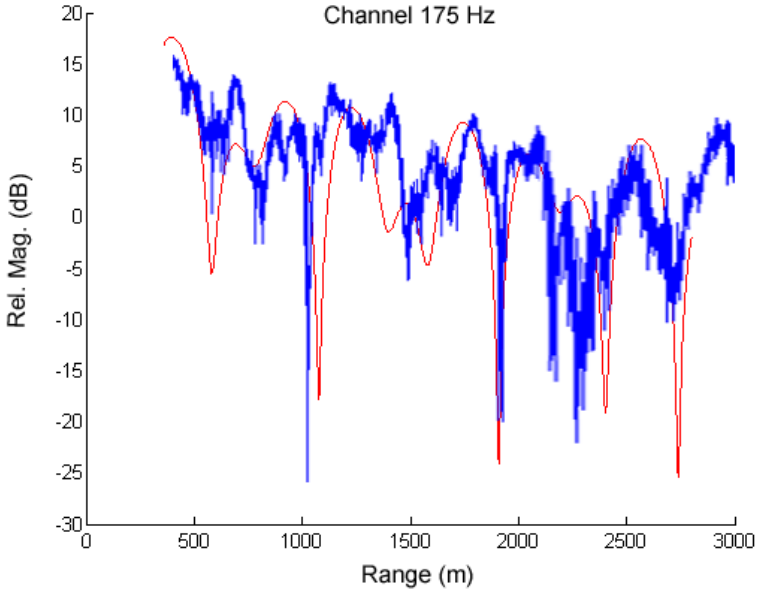

Figure 5.5: Comparison of pressure field magnitude from the inversion (red) and the data (blue) of Curley's 175 Hz Channel

The “no channel” inversions were obtained without the use of limits and the “channel” regions did use limits, but the peaks and valleys of both inversions show about the same amount of agreement with the actual data. The comparisons of pressure field magnitudes are shown at both 75 Hz and 175 Hz to show that this agreement was at both the low end and the high end of the frequency range. This, and the agreement in the mean squared error of the difference in the eigenvalues, shows that the use of limits is a valid method of inversion.

6.0 Application to the Other Buoys

Data from the SW06 experiment were collected on four separate buoys; up to this point, only data from the buoy Curley has been analyzed. To determine if this method is reliable it will have to be tested on data from the other buoys, Moe, Larry, and Shemp, as well.

The firsts step in analyzing these new buoys is to find regions of “Channel” and “No Channel” for each. Maps of the regions traversed by Moe, Larry, and Shemp can be seen in figures 6.1, 6.2, and 6.3 respectively.

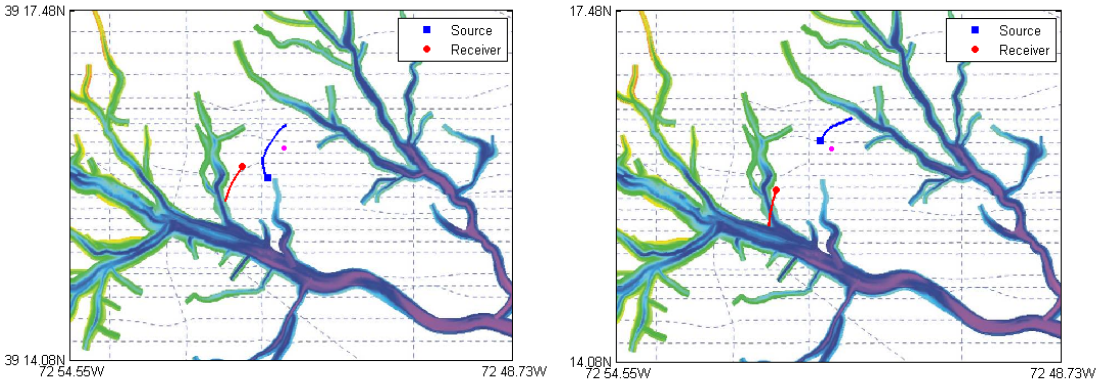

a) b)

Figure 6.1: Map of Moe over a) “No Channel” and b) “Channel”

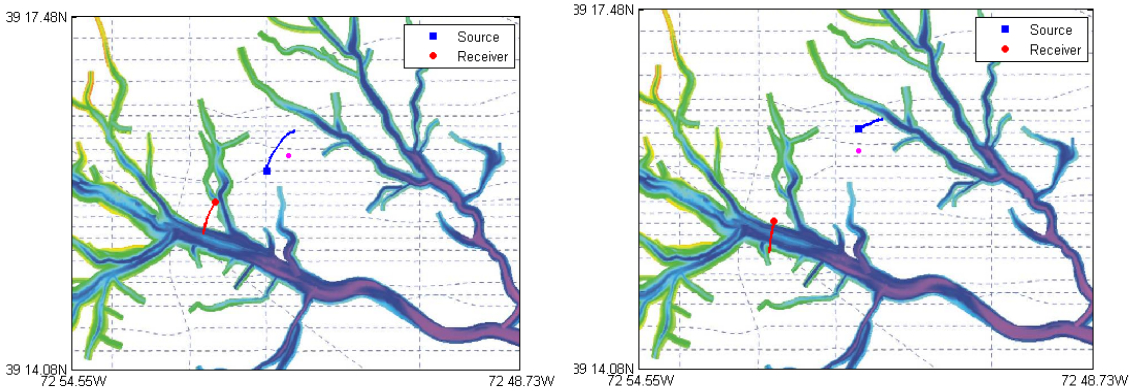

a) b)

Figure 6.2: Map of Larry over a) “No Channel” and b) “Channel”

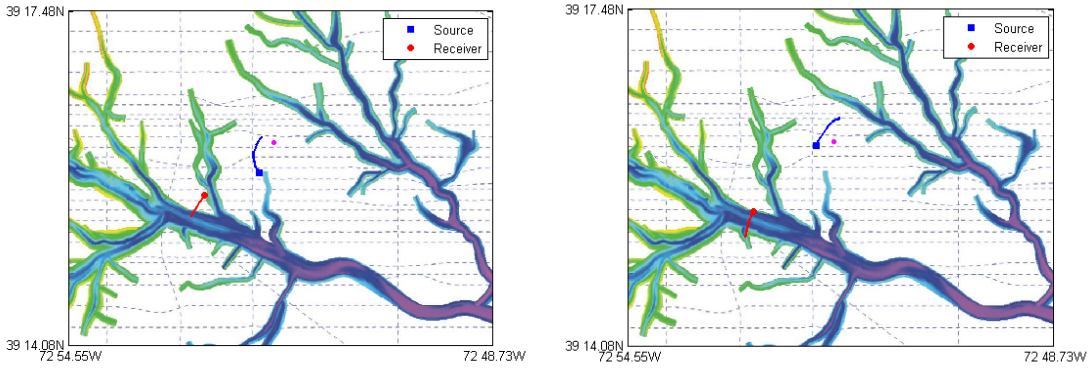

a) b)

Figure 6.3: Map of Shemp over a) “No Channel” and b) “Channel”

6.1 Spectroscopy

Eigenvalues from Moe, Larry and Shemp were successfully obtained for “No Channel” regions from Moe and Larry, and for “Channel” regions from Moe and Shemp. They were collected in the same manner as the eigenvalues from Curley from the autoregressive spectra. After the eigenvalues were obtained by frequency, they were compared to the KRAKEN results to see if any were spurious or outside the acceptable range for each frequency. Since both “Channel” and “No Channel” data were obtained for Moe, they are both shown in the same plots in figure 6.4. Larry’s “No Channel” spectroscopy can be seen in figure 6.5 and Shemp’s “Channel” data can be seen in figure 6.6. In all three sets of spectroscopy the yellow lines are for the actual data from the buoy and the red lines are for the synthetic data from KRAKEN based on the models from the stratigraphy of the area.

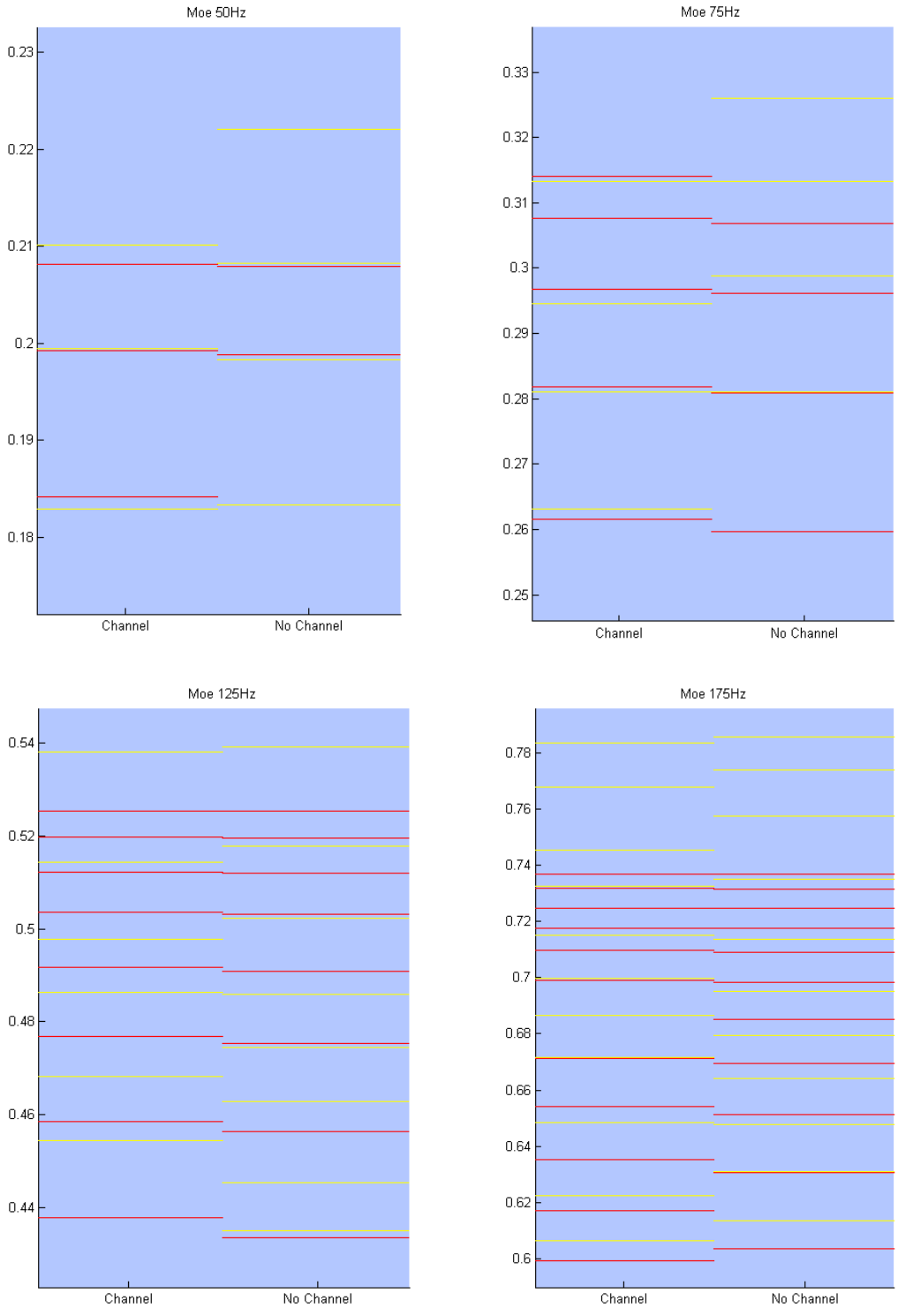

Figure 6.4: Modal Spectroscopy of Moe's eigenvalues

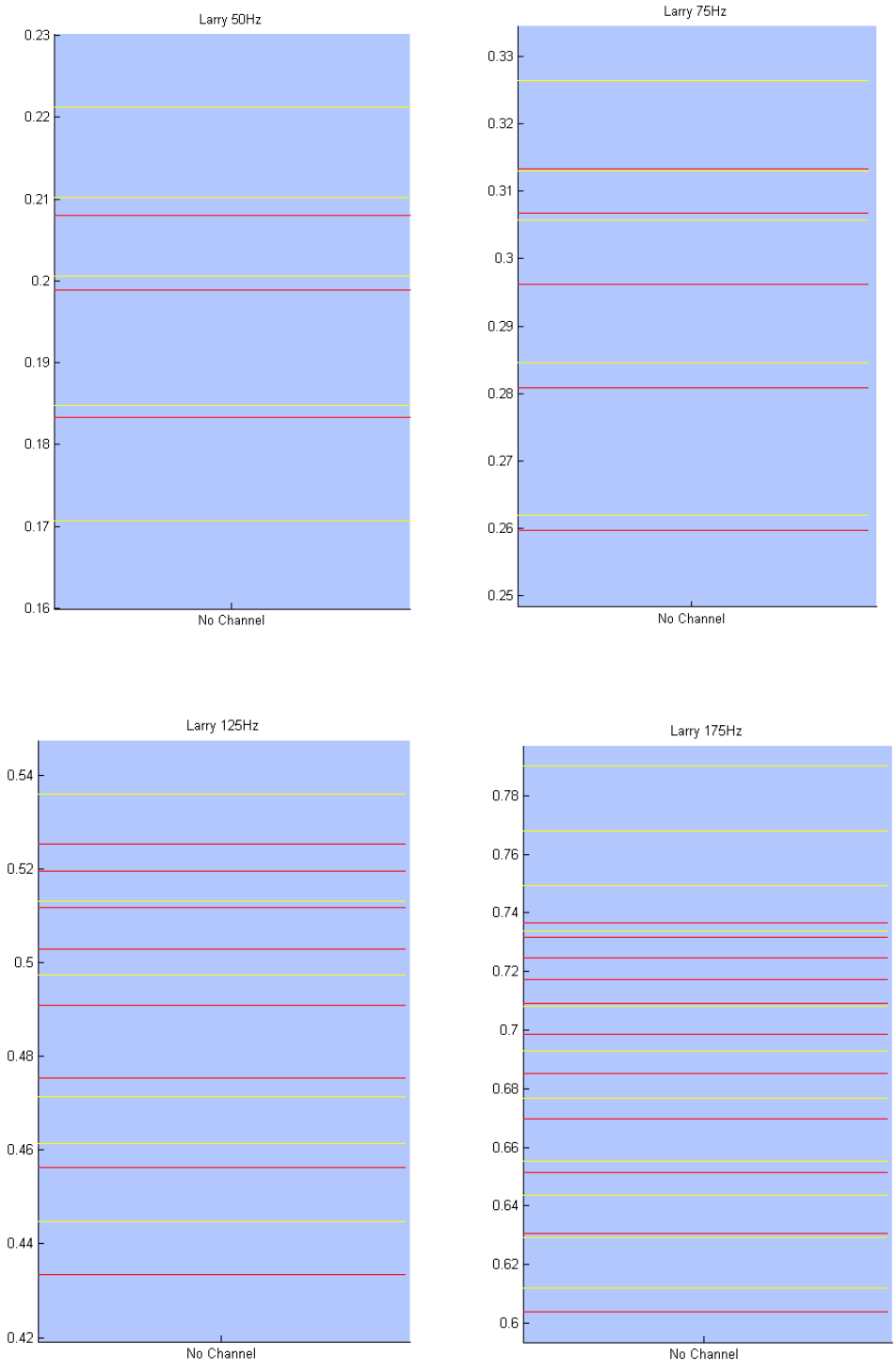

Figure 6.5: Modal Spectroscopy of Larry's eigenvalues

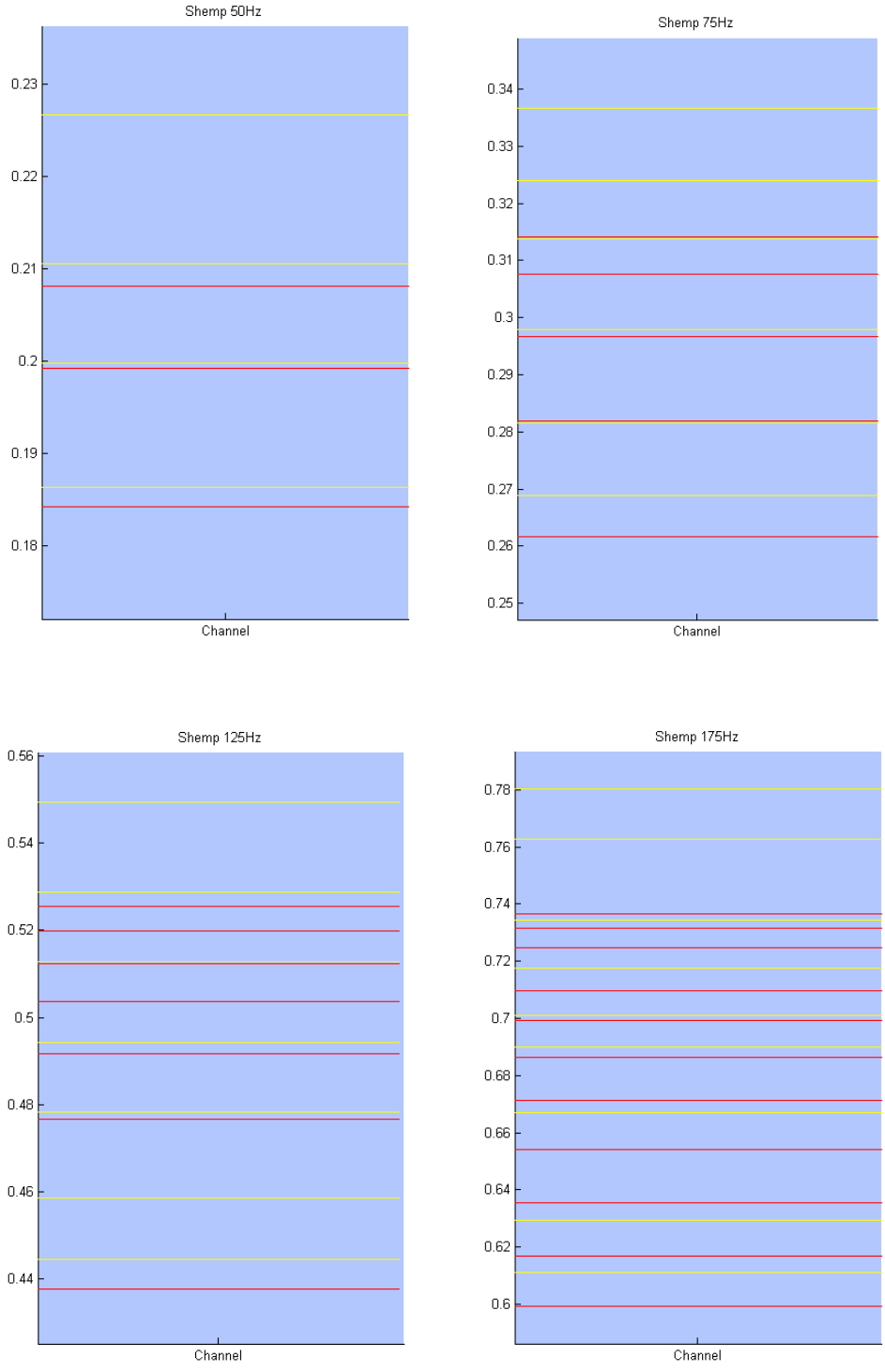

Figure 6.6: Modal Spectroscopy of Shemp's eigenvalues

6.2 Mode Identification

This modal spectroscopy helped again to determine the identification of each mode compared to the KRAKEN results from simulated data and if some of the obtained eigenvalues were results of spurious peaks in the AR data. The mode identification can be seen in Table 6.1.

50Hz

Channel												
	Moe				0.210155	0.199418	0.182927					
	Shemp			0.226646	0.210539	0.199801	0.186379					
	Kraken				0.208117	0.199249	0.184173					
No Channel												
	Moe			0.222044	0.208238	0.198267	0.183311					
	Larry			0.221277	0.210155	0.200568	0.184845	0.170655				
	Kraken				0.207986	0.19884	0.18331					

75Hz

Channel												
	Moe				0.313316		0.294524	0.281102	0.263078			
	Shemp		0.336709	0.324053	0.313699		0.297976	0.281486	0.26883			
	Kraken				0.314034	0.307678	0.296713	0.281917	0.261638			
No Channel												
	Moe			0.325971	0.313316		0.298743	0.281102				
	Larry			0.326354	0.312932	0.305646		0.284553	0.261927			
	Kraken				0.313342	0.306768	0.296148	0.280854	0.259672			

125Hz

Channel												
	Moe		0.538044			0.514267		0.486272	0.468248	0.454442		
	Shemp		0.549549	0.52884		0.512733		0.494325	0.478219	0.45866	0.444471	
	Kraken			0.525448	0.519756	0.512248	0.503567	0.491731	0.476752	0.458523	0.437687	
No Channel												
	Moe		0.539194		0.517719		0.502379	0.485888	0.474384	0.462879	0.434884	
	Larry		0.536126			0.513117	0.497393		0.471316	0.461345	0.444854	
	Kraken			0.525393	0.519573	0.511947	0.50307	0.490868	0.475367	0.456217	0.433452	

175Hz

Channel																	
	Moe		0.783481	0.767757	0.745515		0.732476		0.715219		0.699879		0.6715	0.64849	0.622413	0.606306	
	Shemp			0.780413	0.762772	0.734393			0.71752		0.701029	0.689908	0.666898		0.629316	0.611291	
	Kraken					0.736721	0.731672	0.72474	0.717672	0.709609	0.699144	0.686453	0.671358	0.654205	0.635424	0.616978	0.599158
No Channel																	
	Moe		0.785782	0.773893	0.757403	0.73516			0.713685		0.695277	0.679554	0.664214	0.647723	0.63085	0.613592	
	Larry		0.79	0.767757	0.74935		0.733626			0.707932	0.692976		0.676869	0.655393	0.629316	0.612058	
	Kraken					0.736693	0.731564	0.724534	0.717409	0.709154	0.698429	0.685334	0.669654	0.651489	0.630629	0.603768	

Table 6.1: Mode identification for Moe, Larry, and Shemp eigenvalues

6.3 Inversions

With identified modes it is possible to use these eigenvalues with the inversion program. Since it has already been shown with the Curley data that using multiple frequency data simultaneously is effective, as well as implementing limits on the range of values the points in the sound speed profile are allowed to take, these inversions can be done with these ideas already in place. Inversions using multiple frequency data and constraints on sound speed for “No Channel” for Moe and Larry and “Channel” for Moe and Shemp can be seen in figures 6.7-10 in which the blue line is the inversion, the red line is the assumed profile and the green line is the background for the inversion.

The paths of each of the buoys are shown in figure 6.11 in which it is shown that Moe, Larry, and Shemp traveled roughly the same path compared to Curley whose path varied greatly from the others; each of these areas are boxed in the figure. Because Moe, Larry, and Shemp were in close proximity it can be assumed that the stratigraphy of the “No Channel” and “Channel” regions would be very similar to the “No Channel” and “Channel” regions of each of the other buoys. However, since Curley was in a slightly different region, the stratigraphy cannot be assumed to be the same as the others. This can account for the fact that the inversions do not match perfectly to the assumed truth. The assumed profile for each region was based on the stratigraphy of the area Curley traveled over, not Moe, Larry, and Shemp.

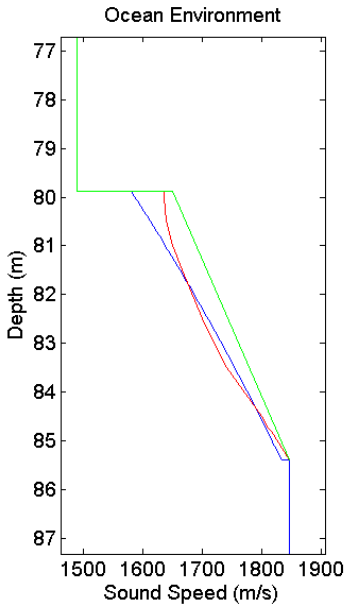

Figure 6.7: “No Channel” inversion for Moe (blue), background (green), and assumed profile (red)

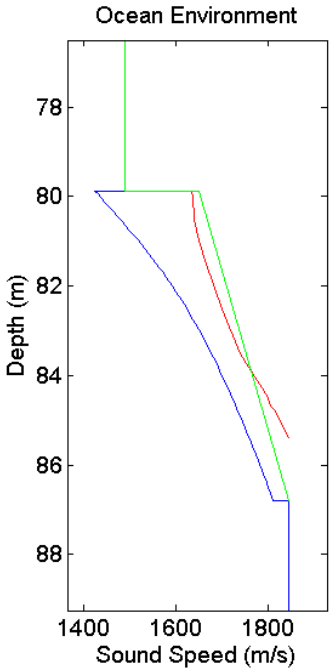

Figure 6.8: “No Channel” inversion for Larry (blue), background (green), and assumed profile (red)

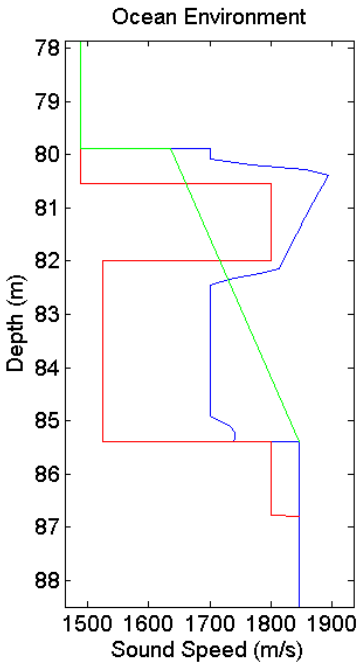

Figure 6.9: “Channel” inversion for Moe, (blue), background (green), and assumed profile (red)

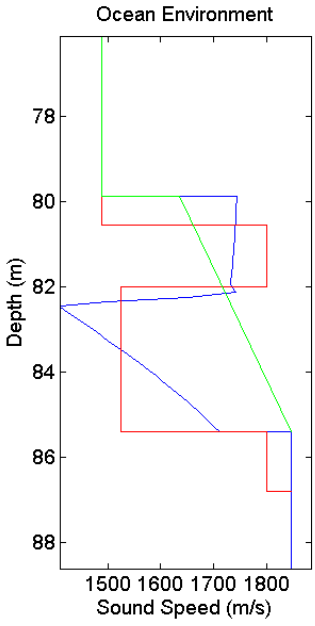

Figure 6.10: “Channel” inversion for Shemp (blue), background (green), and assumed profile (red)

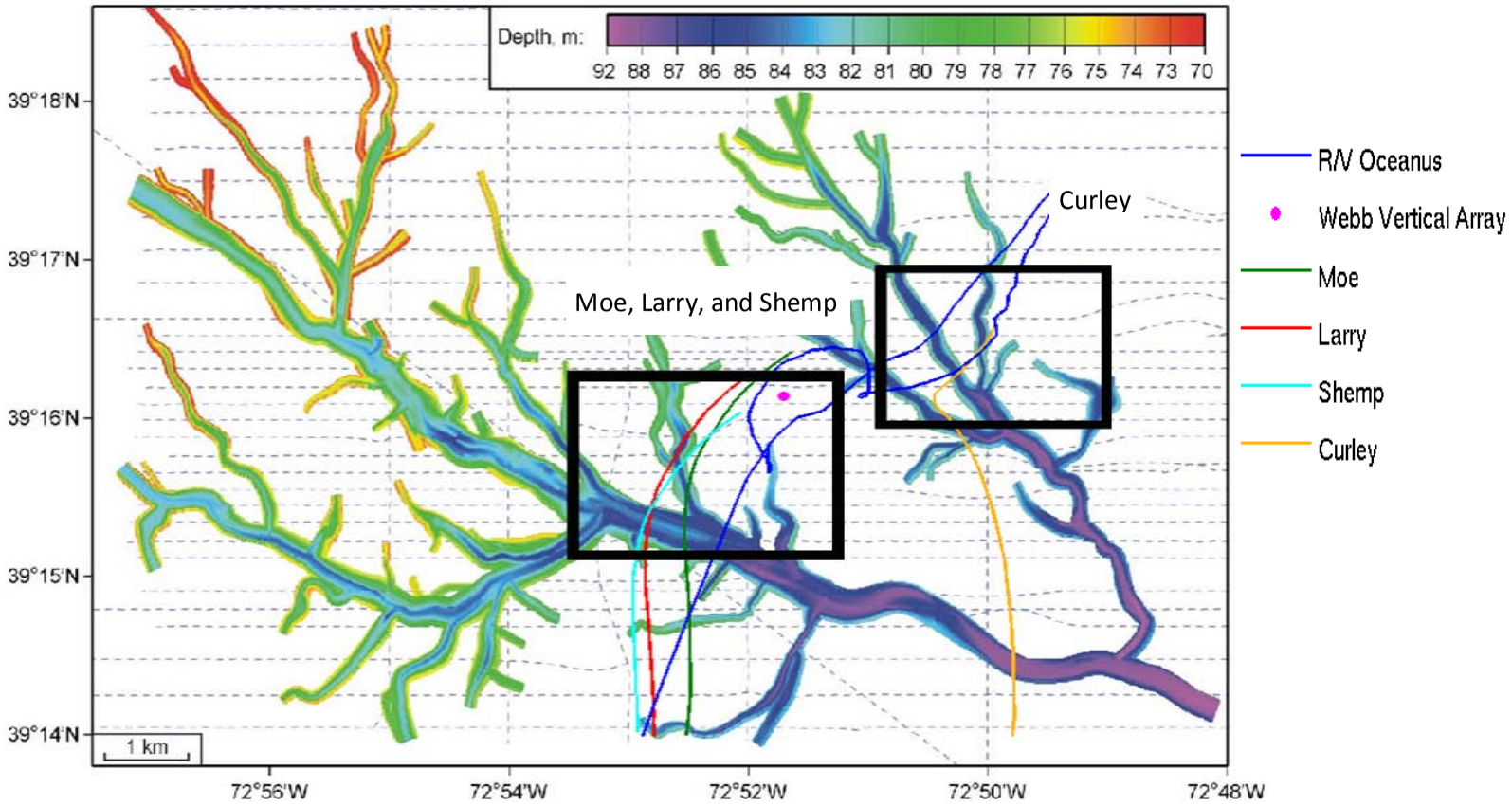

Figure 6.11: Paths of buoys

7.0 Conclusions and Suggestions for Future Work

The goal of this work was to determine an accurate method of geoacoustic inversion using data from multiple frequencies. Accurate models of the sound speed profile in both the “channel” and “no channel” regions will help to determine how the subbottom channels affect the sound propagation.

By breaking the Curley buoy data into regions of “channel” and “no channel”, it has been seen that the two areas are significantly different by comparing their eigenvalues and the resulting profiles when those eigenvalues are used in an inversion program. The inversion program proved to be a successful tool, especially when using multiple frequencies simultaneously and constraints were put on the range of acceptable sound speed values.

7.1 Stratigraphy

These ideas were also applied to the data from the other buoys involved in the experiment, although they were not entirely successful because the inversion did not perfectly match the model based on the stratigraphy. A suggestion for continuing this line of work would be to obtain the stratigraphy of the exact locations of the new “channel” and “no channel” regions to use as an assumed profile in the inversions to determine if these are more acceptable than using the stratigraphy of Curley’s “channel” and “no channel” regions.

7.2 Patterns in Modal Spectroscopy

An area of interest that this work did not deal with, but would be useful, is to look for patterns in the modal spectroscopy. One pattern that was noticed in the Curley data was that the second mode at each frequency is consistently missing in the spectroscopy. Patterns such as this could help to predict what eigenvalues will be obtained in similar locations. It will also help when the sediment environment is unknown to determine if it could be a region with subbottom channels.

7.3 Qualitative Regularization

The next major step in this work will be to use the Qualitative Regularization method of inversion. This method allows the inversion program to perturb around known discontinuities, which are included in the models based on the stratigraphy. This method will allow the solution to be piecewise smooth, but also incorporates the Heaviside step function for the discontinuities.

The perturbative inversion program is a method used to solve a problem that is both ill-posed and underdetermined [45]. It is ill-posed because small errors in the data can cause large errors in the solution, and because there is the possibility of an infinite number of least squares solutions to one problem. It is underdetermined because the equation calls for a continuous function of sound speed with depth, but the models provide only speeds at discrete depths. These two issues have often been handled by setting a constraint such that the smoothest profile is the one chosen as the best fit. Methods that have successfully implemented this constraint are SVD and Tikhonov Regularization [10, 25-6, 38, 39, 40].

Due to geological processes, sediments are often better described by layers with distinct properties rather than being represented by a smooth profile. In cases such as this, both SVD and Tikhonov regularization result in a smoothed version of the true profile. A method has been developed that utilizes knowledge of locations of discontinuities in sediment layers to constrain the solution and resolve discontinuities in the sediment sound speed profile to provide a better result. Qualitative Regularization can be applied to the sediment inverse problem in order to incorporate discontinuities in the sound speed profile [34]. Qualitative regularization removes the effect of regularization by allowing a discretized Heaviside step function at a specified location which incorporates a jump with no constraint on the size or direction. The jump may be positive, negative, or remain the same [45].

When inverting for the sediment sound speed profile independently, the water column sound speed profile is assumed to be known. If this assumption is not entirely correct, the sediment profile will also be incorrect because it will be compensating for the error in the water column [27, 41, 45]. If knowledge of the water column sound speed profile is poor, the effect will be significant errors in the estimation of the sediment properties [27, 28]. Qualitative Regularization has solved this issue by inverting simultaneously for the sound speed profiles of the water column and the sediment. Because the values at the very top and very bottom of the sound speed profile in the water column can vary greatly due to the variable temperature at the surface and the assumed properties of the water-bottom interface, the inversion of the water column uses the method of approximate equality constraints in which the two shallowest and two deepest depths of the water sound speed profile are approximated to the trajectory of the rest of the profile [35, 45].

Qualitative Regularization can hold up well to inaccurate data. When wavenumbers are poorly estimated, this method can still obtain accurate results by increasing the Lagrange multiplier, which places less emphasis on the data and more weight on the knowledge of discontinuities [45]. However, when incorrect inputs for the sound speed discontinuities are used in the inversion, the solution will reflect this. In addition to having the discontinuities in the wrong locations, the solution will differ from the true profile by having different sound speed values in each layer. This is because the result is a layered profile with the sound speeds in each layer being the weighted average of the true speeds integrated over the depths of the layers.

REFERENCES

[1] Frisk, G. V. (2009) “Modal Mapping Techniques for Geoacoustic Inversion and Source Localization in Laterally Varying, Shallow-Water Environments,” ONR Annual Report.

[2] Ballard, M. S., K. M. Becker, and J. A. Goff (2010) “Geoacoustic Inversion for the New Jersey Shelf: Three Dimensional Sediment Model”, *IEEE Journal of Oceanic Engineering*, 35(1), pp. 28-42.

[3] Ratilal, P., Y. Lai, D. T. Symonds, L. A. Ruhlmann, J. R. Preston, E. K. Scheer, M. T. Garr, C. W. Holland, J. A. Goff, and N. C. Makris, (2005) “Long range acoustic imaging of the continental shelf environment: The Acoustic Clutter Reconnaissance Experiment 2001,” *Journal of the Acoustical Society of America*, 117(4), pp. 1977-98.

[4] Goff, J. A. (2006) Private Communication.

[5] Frisk, G.V., and K.M. Becker (2000) “Modal Evolution and Inversion in Laterally Varying, Shallow-Water Waveguides,” *Proceedings of the International Conference on Acoustics, Noise and Vibration*, Montreal, Quebec, Canada.

[6] Frisk, G. V. (1994) *Ocean and Seabed Acoustics: A Theory of Wave Propagation*, Prentice Hall, Englewood Cliffs, New Jersey.

[7] Frisk, G. V. (1995) "A Review of Modal Inversion Methods for Inferring Geoacoustic Properties in Shallow Water," invited paper in *Full Field Inversion Methods in Ocean and Seismo-Acoustics*, edited by O. Diachok, A. Caiti, P. Gerstoft, and H. Schmidt, Kluwer, Netherlands.

[8] G. V. Frisk (1990) “Inverse Methods in Ocean Bottom Acoustics,” *Oceanographic and Geophysical Tomography*, edited by Y. Desaubies, A. Tarantola, and J. Zinn-Justin, Elsevier Science Publishing Co., New York.

[9] Becker, K. M. (2002) “Geoacoustic Inversion in Laterally Varying Shallow-Water Environments Using High-Resolution Wavenumber Estimation,” Ph.D. Thesis, MIT/WHOI Joint Program in Oceanography/Applied Ocean Science and Engineering, Cambridge, MA and Woods Hole, MA.

[10] Rajan, S. D., J. F. Lynch, and G. V. Frisk, (1987) ”Perturbative Inversion Methods for Obtaining Bottom Geoacoustic Parameters in Shallow Water,” *Journal of the Acoustical Society of America,* 82(3), pp. 998-1017.

[11] Souza, L. L. (2005) “Inversion for Subbottom Sound Velocity Profiles in the Deep and Shallow Ocean,” Ph.D. Thesis, MIT/WHOI Joint Program in Oceanography/Applied Ocean Science and Engineering, Cambridge, MA and Woods Hole, MA.

[12] Sakai, H. (1979) “Statistical Properties of AR Spectral Analysis,” *IEEE Trans. Acoust., Speech, Signal Processing,* ASSP-27(4).

[13] Marple Jr., S. L. (1987) *Digital Spectral Analysis with Applications,* Prentice Hall, Englewood Cliffs, New Jersey.

[14] Ohta, K., K. Okabe, I. Morishita, G.V. Frisk, and A. Turgut, (2009) “Modal Inversion Analysis for Geoacoustic Properties of the New Jersey Continental Shelf in the SWAT Experiments,” *IEEE J. Oceanic Engineering*, 34(4), pp. 526-538.

[15] Rajan, S. D., G. V. Frisk, K. M. Becker, J. F. Lynch, G. Potty, and J. H. Miller (2008) “Modal Inverse Techniques for Inferring Geoacoustic Properties in Shallow Water,” *Important Elements in: Geoacoustic Inversion, Signal Processing, and Reverberation in Underwater Acoustics*, edited by A. Tolstoy, Research Signpost, Kerola, India.

[16] Goff, J. (2009) Private communication, 2009.

[17] Tolstoy, I. and C. S. Clay, (1987) “Ocean Acoustics: Theory and Experiment in Under-water Sound,” American Institute of Physics, New York, NY.

[18] Clay, C. S. and H. Medwin (1977) *Acoustical Oceanography: Principles and Applications*, John Wiley, New York, NY.

[19] Porter, M. B. (1991) “The KRAKEN normal mode program”, Technical report, SACLANT Undersea Research Center, La Spezia, Italy.

[20] Etter, P. C. (2003) *Underwater Acoustic Modeling and Simulation*, Spon Press.

[21] Holland, C. W. and J. Osler (2000) “High resolution geoacoustic inversion in shallow water: A joint time and frequency domain technique," *Journal of the Acoustical Society of America*, 107(3), pp. 1263-1279.

[22] Fallat, M. R. and S. E. Dosso (1999) “Geoacoustic inversion via local, global, and hybrid algorithms," *Journal of the Acoustical Society of America*, 105(6), pp. 3219-3230.

[23] Frisk, G. V. and J. F. Lynch (1984) “Shallow water waveguide characterization using the Hankel transform," *Journal of the Acoustical Society of America*, 76(1), pp. 205-216.

[24] Becker, K. M. and G. V. Frisk (2006) “Evaluation of an autoregressive spectral estimator for modal wavenumber estimation in range dependent shallow water waveguides," *Journal of the Acoustical Society of America*, 120(3), pp. 1423-1434.

[25] Frisk, G. V., J. F. Lynch, and S. D. Rajan (1989) “Determination of compressional wave speed profiles using modal inverse techniques in a range dependent environment in Nantucket Sound," *Journal of the Acoustical Society of America*, 86(5), pp. 1928-1939.

[26] Ohta, K. and G. V. Frisk (1997) “Modal Evolution and Inversion for Seabed Geoacoustic Properties in Weakly Range-Dependent Shallow Water Waveguides," *IEEE Journal of Ocean Engineering*, 22(3), pp. 501-521.

[27] Lin, Y.-T., C.-F. Chen, and J. F. Lynch (2006) “An Equivalent Transform Method for Evaluating the Effect of Water-Column Mismatch on Geoacoustic Inversion," *IEEE Journal of Ocean Engineering*, 31(2), pp. 284-298.

[28] Snellen, M., D. G. Simons, M. Siderius, J. Sellschopp, and P. L. Nielsen (2001) “An evaluation of the accuracy of shallow water matched field inversion results," *Journal of the Acoustical Society of America*, 109(2), pp. 514-527.

[29] Goff, J. A., J. A. Austin Jr., S. Gulick, S. Nordfjord, B. Chistensen, C. Sommerfield, H. Olson, and C. Alexander (2005) “Recent and modern marine erosion on the New Jersey outer shelf," *Marine Geology*, 216, pp. 275-296.

[30] Apel, J. R., M. Badiey, C.-S. Chiu, S. Finette, R. Headrick, J. Kemp, J. F. Lynch, A. Newhall, M. H. Orr, B. H. Pasewark, D. Tielbuerger, A. Turgut, K. von der Heydt, and S. Wolf (1997) “An overview of the 1995 SWARM shallow water internal wave acoustic scattering experiment," *IEEE Journal of Ocean Engineering*, 22(3), pp. 465-500.

[31] McClennen, C. E. (1973) *Nature and the origin of the New Jersey continental shelf topographic ridges and depressions*, Ph.D. thesis, University of Rhode Island.

[32] Davies, T. A., J. A. Austin Jr., M. B. Lagoe, and J. D. Milliman (1992) “Late Quarternary sedimentation off New Jersey: New results using 3-D seismic profiles and cores," *Marine Geology*, 108, pp. 323-343.

[33] Goff, J. A., B. J. Kraft, L. A. Mayer, S. G. Schock, C. K. Sommerfield, H. C. Olson, S. P. S. Gulick, and S. Nordfjord (2004) “Seabed characterization on the New Jersey middle and outer shelf: Correlability and spatial variability of seafloor sediment properties," *Marine Geology*, 209, pp. 147-172.

[34] Simcik, L. and P. Linz (1994) *Qualitative Regularization: Resolving Non-smooth Solutions, Tech. Rep. CSE-94-12*, University of California, Department of Mathematics.

[35] Medeiros, W. E. and J. B. C. Silva (1996) “Geophysical inversion using approximate equality constraints," *Geophysics*, 61(6), pp. 1678-1688.

[36] Jensen, F. B., W. A. Kuperman, M. B. Porter, and H. Schmidt (1994) *Computational Ocean Acoustics*, American Institute of Physics.

[37] Weston, D. E. (1971) “Intensity-range relations in oceanographic acoustics," *Journal of Sound and Vibration*, 18(2), pp. 271-287.

[38] Menke, W. (1989) Geophysical Data Analysis: Discrete Inverse Theory, vol. 45 of *International Geophysics Series*, Academic Press.

[39] Aster, R. C., B. Borchers, and C. H. Thurber (2005) *Parameter Estimation and Inverse Problems*, Elsevier.

[40] Lynch, J. F., S. D. Rajan, and G. V. Frisk (1991) “A comparison of broadband and narrow-band modal inversions for bottom geoacoustic properties at a site near Corpus Christi, Texas," *Journal of the Acoustical Society of America*, 89(2), pp. 648-665.

[41] Dosso, S. E. and P. L. Nielsen (2002) “Quantifying uncertainty in geoacoustic inversion. II. A fast Gibbs sampler approach," *Journal of the Acoustical Society of America*, 111(1), pp. 143-159.

[42] Ballard, M. S. and K. M. Becker (2008) “Geoacoustic inversion on the New Jersey margin: Along and across the shelf," *Journal of the Acoustical Society of America*, 124(3), pp. EL141-EL145.

[43] Matsumoto, S. and K. Ohta (2004) “Study on Range-Dependant Evolution of Mode Eigenvalue by Using the Wigner Distribution Function," *Japanese Journal of Applied Physics*, 43(5B), pp. 3127-3130.

[44] Becker, K. M., S. D. Rajan, and G. V. Frisk (2003) “Results from the Geoacoustic Inversion Techniques Workshop using Modal Inverse Methods," *IEEE Journal of Ocean Engineering*, 28(3), pp. 331-341.

[45] Ballard, M. S. (2009) *Optimized Constraints for the Linearized Geoacoustic Inverse Problem*, Ph.D. thesis, Pennsylvania State University.